TD-04-043
12/04

MEASUREMENTS OF GEOMETRIC, HYSTERETIC AND DYNAMIC SEXTUPOLE IN TEVATRON DIPOLES

G. Annala, G. Ambrosio, P. Bauer, L. Bottura*, R. Carcagno, J. DiMarco, R.W. Hanft, M.J. Lamm, M. Martens, P. Schlabach, C. Sylvester, M. Tartaglia, J.C. Tompkins, G. Velev

Fermilab
* CERN/AT

Beam loss and emittance dilution during ramping from injection to collision energy is observed in the Tevatron, now in its collider run-II stage. Imperfect control of the machine chromaticity during the injection porch and the ensuing ramp to collision could contribute to the beam loss. Dipole magnets are the main source of chromaticity in the Tevatron. Sextupole correctors are distributed around the ring to compensate for the sextupole from the dipole magnets. Furthermore, the sextupole component in the superconducting Tevatron dipole magnets decays during the injection plateau and snaps back to the value before the start of the decay at the start of the ramp. The chromaticity correctors also correct for this so-called dynamic sextupole behavior.

To determine if the sextupole compensation is working successfully in the Tevatron a thorough investigation of the sextupole (b_2) in Tevatron dipole magnets was recently conducted. This included an extensive series of off-line magnetic measurements on several Tevatron dipole magnets from the spare pool. Traditionally one differentiates between three different b_2 components, geometric, hysteretic and dynamic. This note discusses the results of these measurements.

The experiments were also complemented with magnetic field calculations and analysis of data from the Tevatron magnetic measurement archive. On the basis of this document it is hoped that the chromaticity correction scheme in the Tevatron can be improved. Such improvements, however, are discussed in a separate note on the Tevatron chromaticity compensation (TD-03-008 – Revision I). This work is essentially a continuation of a similar study conducted in 1996 [1], on the basis of which the chromaticity correction scheme for the Tevatron run II was devised.

Table of Contents

1) Introduction ... 3
1.1) The Tevatron Dipole Magnets ... 3
1.2) Components of the Sextupole in Tevatron Dipoles ... 3
1.3) Discovery and Previous Studies of Drifting Sextupoles in Tevatron Dipoles ... 5
1.4) Rationale for the Recent Tevatron b2 Studies ... 7
1.5) Dynamic Effects in Superconducting Magnets – General Introduction ... 7
1.6) Tevatron Dipole Magnet Study Program ... 8
1.7) Magnetic Measurement Systems ... 9
1.7.1 Rotating Coil Measurement System ... 11
1.7.2 Hall Probe Measurement System ... 13
1.8) Magnetic Measurement Procedure and Current Cycle ... 14
2) Geometric b2 ... 18
2.1) Tevatron Magnetic Measurement Archive Data ... 18
2.2) Magnetic Models of the Tevatron Dipole ... 20
2.3) Recent Measurements ... 21
2.4) Z-Scan – End Measurements and b2 Variation Along Body ... 22
2.5) b2 Pattern ... 24
3) Hysteretic b2 ... 26
3.1) Hysteretic - Archive Data ... 26
3.2) Summary – Recently Measured b2 Loops ... 27
3.3) End-Body ... 31
3.4) Temperature Effect ... 32
3.5) Eddy Current Effect ... 33
4) Dynamic b2 ... 35
4.1) Analysis Procedures ... 35
4.2) Drift ... 36
4.2.1 Parametrization of the b2 dependence on time ... 36
4.2.2 Decay amplitude vs duration of flattop ... 37
4.2.3 Decay amplitude vs duration of backporch ... 38
4.2.4 Decay amplitude vs number of flattops ... 39
4.2.5 Decay amplitude vs the maximum flattop current ... 40
4.2.6 Decay amplitude vs duration of frontporch ... 41
4.2.7 Comparison of the decay in body vs end and body vs body ... 42
4.2.8 Temperature dependence of the decay ... 43
4.2.9 Special case: FT 60 min, BP 5 min and variable IP ... 43
4.3) Snap-back ... 45
4.3.1 Parametrization of the snapback amplitude ... 45
4.3.2 Snapback amplitude and time vs duration of flattop ... 46
4.3.3 Snapback amplitude and time vs duration of backporch ... 47
4.3.4 Snapback amplitude and time vs number of flattops ... 48
4.3.5 Snapback amplitude and time vs maximum flattop current ... 50
4.3.6 Snapback amplitude and time vs duration of frontporch ... 50
4.3.7 Comparison of the snapback for different longitudinal positions ... 51
4.3.8 Special case: snapback at FT = 60 min and variable BP duration ... 52
4.3.9 Comparison of Hall-probe and Rotating Coil Measurements ... 53
4.4) Summary of the Effect of Powering History on Drift and Snapback ... 53
4.5) Correlation between the Snapback Amplitude and Time ... 54
5) Conclusions ... 56
References ... 58
APPENDIX 1 ... 59

1) Introduction

1.1) The Tevatron Dipole Magnets

The Tevatron proton antiproton collider operates since 1983 and is currently in its collider run-II stage. The Tevatron lattice consists mainly of *774* six meter long superconducting arc dipole magnets and *180* superconducting arc quadrupole magnets to accelerate and store proton and antiproton beams at *980 GeV*. Figure 1 shows a cross sectional view of a Tevatron dipole magnet. The main features of this magnet are –1- a two-layer, wedge-less cosine-theta coil design, -2- a three inch bore diameter, -4- a warm iron yoke, -5- a compact, multi-layer cryostat assembly around the stainless steel collars, -6- four diagonal bolts that support the cryostated coils within the warm iron yoke in the nine so-called suspension stations along the magnet.

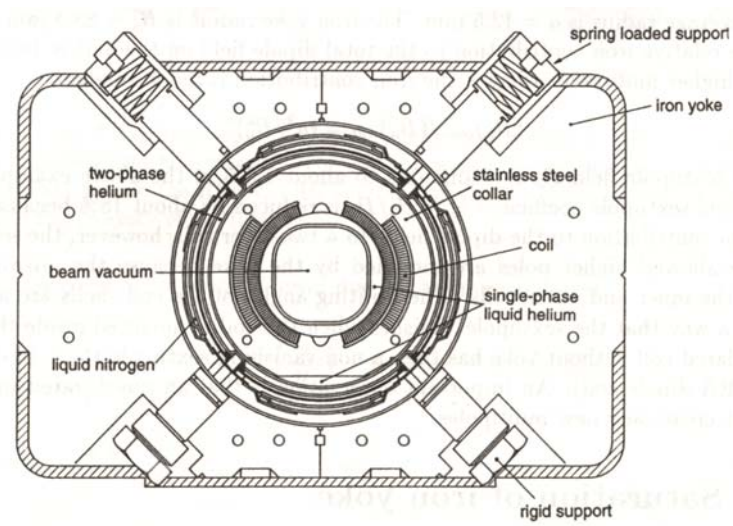

Figure 1: Tevatron dipole cross-section in supports section.

1.2) Components of the Sextupole in Tevatron Dipoles

As the leading higher harmonic in a dipole magnet, the sextupole field component (b_2) is typically the most important field error. Throughout this document the b_2 component will be given in units of the main dipole field B_0. One unit of b_2 corresponds to a sextupole field strength at the so-called reference radius of 10^{-4} times that of the dipole field in the straight section. The reference radius is arbitrarily defined as one inch (*25.4 mm*). Note that this convention also applies to the end field measurements where the raw multipole data need to be renormalized to the body-field with the ratio of average end field, $B_{0,end}$, to the body field, $B_{0,body}$. The average end field depends on what section of the coil is defined as end (or how long the measurement probe is). This document discusses the *geometric*, *hysteretic* and *dynamic* b_2 components separately.

The ***geometric*** b_2 component is defined as the component produced directly by the current distribution in the coils, as it would be produced for example by a coil wound from cables made of copper (assuming that the copper could carry as much current as a superconductor, which of course it can't). The geometric contribution also includes the field contribution of the iron yoke, although often iron saturation effects are also differentiated from the geometric multipole contribution. The Tevatron dipole magnet uses a so-called warm yoke design in which iron saturation effects are small (order *~0.1 units* of b_2). This and other specifics of the geometric sextupole component in Tevatron dipoles will be discussed in chapter 2.

The ***hysteretic*** b_2 component is current dependent and the result of magnetization in the superconductor. There is also a contribution from eddy currents induced on the ramp, but this effect gives a negligible contribution to the b_2 in Tevatron dipole magnets *(< 0.1 units*). In Tevatron dipoles the hysteretic component is of the order of several units. As the magnetization effect is "squeezed" out at higher currents the hysteretic loop narrows and the only remaining contribution is the geometric multipole. Usually the hysteresis loop is more or less symmetric around the geometric multipole. This and other specifics of the hysteretic sextupole component in Tevatron dipoles will be discussed in chapter 3.

The ***dynamic*** b_2 component consists of a drift of the multipole during fixed current operation in the magnets, followed by a so-called snapback at the start of an ensuing ramp. It is well known that the b_2 component in the superconducting dipole magnets in the Tevatron decays by approximately one to two units during the injection plateau since these effects were first discovered in the Tevatron (see a brief recapitulation of this discovery below). The multipole drift is believed to be the result of superconductor demagnetization effects caused by current redistributions within the superconducting cables from which the coils are wound. These current redistributions are always present in superconducting coils and can be influenced by the contact resistance between strands within the cable as well as in the splices and by the magnet end design. They typically consist of different components with different decay scales. Their presence can also be seen in the bore field, where they cause the so-called periodic pattern, a periodic modulation by several units of the allowed multipoles along the length of the magnet with the cable twist pitch as period. The dynamic effects depend on the powering history of the magnet and become stronger the larger the superconductor magnetization. This and other specifics of the dynamic b_2 component in Tevatron dipoles will be discussed in chapter 4. The measurements of the dynamic sextupole in Tevatron dipoles was performed not only with rotating coils, but also with a special Hall probe sextupole array supplied by CERN.

Figure 2 illustrates the above said with the case of a measurement of b_2 as function of beam energy (or magnet current) measured in a particular Tevatron dipole. As explained above, the hysteretic loop winds around the geometric b_2 (here *~7.5 units*), while a drift and snapback behavior appears during the dwell on the injection- and back-porches (*150 GeV*).

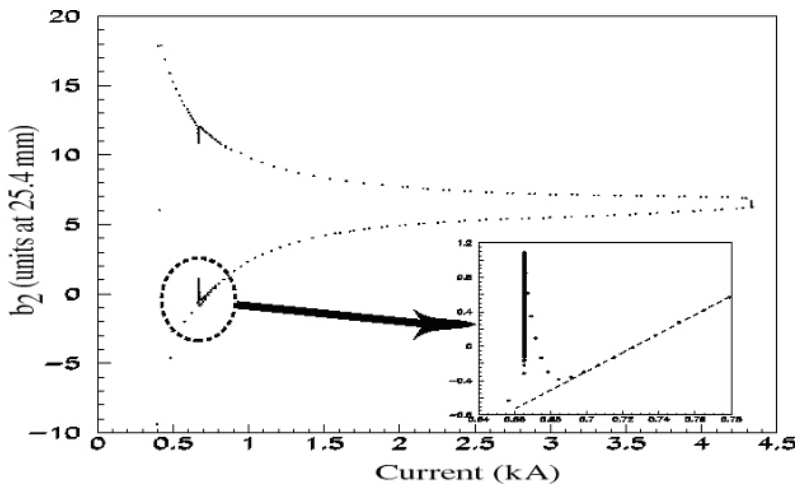

Figure 2: Example of b_2 (at 25.4 mm radius) drift and snapback in Tevatron dipole. The right plot zooms into the drift and snapback during and after injection. The linear extrapolation of the ramp to compute the "hysteretic baseline" is also shown in the insert.

1.3) Discovery and Previous Studies of Drifting Sextupoles in Tevatron Dipoles

During the initial operation of the Tevatron in the collider mode, unexpected chromaticity variations of up to *70 units* were observed during the dwell at injection, [2]. The variations of the tunes and chromaticities appeared to depend on the operational history of the machine. It was quickly found that the cause of this drift was originating within the magnets. Since *25 units* of chromaticity in the Tevatron correspond approximately to one unit of b_2 in the dipole magnets, the above effect was found to be consistent with a b_2 variation of more than two units in each dipole. Following this discovery, a feed-forward b_2 drift compensation was implemented in the Tevatron (the snapback compensation was introduced later). It was also decided at that time to run six pre-cycles to flat-top before beam injection in order to prevent variations of the b_2-drift due to "history effects".

In the following years the issue of drifting sextupole fields was regularly revisited, either to adapt to changes in the accelerator protocol or to advance the understanding of dynamic effects. An example of such measurements is the campaign of 1992. As a result of a change in ramp protocol (one RF unit failed) the Tevatron was plagued by a *10-60%* beam loss at the start of the ramp due to imperfect snapback compensation. A measurement campaign was launched to provide the new compensation fit needed to cope with the modified ramp sequence [3]. Magnetic measurements were performed on five magnets at the Technical Division's Magnet Test Facility (MTF) with rotating coils. Figure 3 shows some snapbacks recorded in this campaign. The 1992 MTF magnetic measurement campaign concluded -1- that there is a 40% magnet-to-magnet spread in decay slopes (*±20%* within one magnet); -2- that during a *30 min* injection porch a drift over *~1.2 units* occurs in TB 353 and approximately two units in TB1207; -3- that the

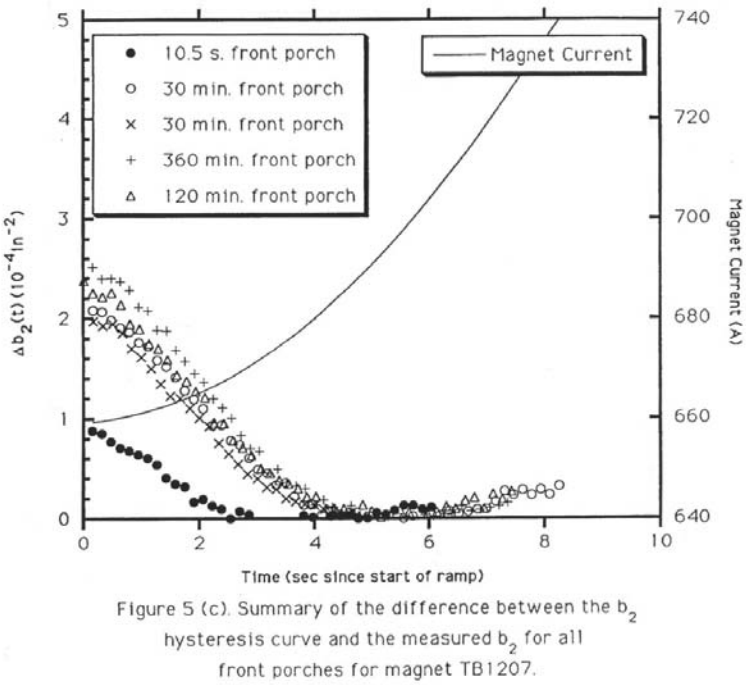

Figure 3: Collection of b_2 snap-backs measured on TB353 (?) for various injection porch durations. Also shown is the current ramp (corresponding to the 1994 Tevatron ramp protocol). Note that the hysteretic and geometric b_2 were not removed from the data and that the fact that the b_2 snaps back to zero is the result of an arbitrary shift of the data. Plot taken from [3].

snapback takes four seconds (which for the particular ramp used then, corresponds to a change in magnet current/field by *~15A/15mT*) and -4- that older data were confirmed which indicated that six pre-ramps are effective in eliminating history dependence [3].

Table 1 summarizes the dynamic effect measurement campaigns preceding the one described in this note. These studies are described in further detail in [4].

Table 1: List of Tevatron magnet dynamic effect measurements.

Year	Magnet	Purpose of Study
87	AA1001 (1m)	discovery of drift
88/89	RL1001 (1m)	discovery of snapback
88/89	TB447, TB223, TB271, TC1194, TB338, TC537, TC1200	remnant field in full length dipoles, drift found also in other multipoles
92	TB353, TB1220, TB1207, TB492, TB862	new Tevatron ramp protocol, first full length magnet measurements
96	TC1052, TB504	back-porch, flat-top energy, preparation for run II
02/03/04	TC1220, TB834, TB438, TC269, TB1052, TB1055, TC0525, TC0710, TB1198, TB1077, TC1130	tune and coupling drift, need for improved b_2 compensation in view of ultimate luminosity, B_0 and b_4 drift, re-shimming demonstration, broken anchor study

1.4) Rationale for the Recent Tevatron b2 Studies

Ten percent (or more) beam loss during ramp from injection to collision, such as reported for instance in [5] and [6], is believed to be mostly the result of beam instabilities, [7], [8]. It is possible, however, that small inaccuracies in the b_2 snapback compensation exacerbate beam instabilities and thus contribute to the beam loss. Beam based measurements of the average b_2 in the magnets have given indications that there is room for improvement in the b_2 feed-forward algorithm in the Tevatron. This and some proposals for possible improvements are discussed in [9].

The study of b_2 properties of several Tevatron dipole magnets presented here represents the basis for any further analysis of the quality and accuracy of the Tevatron b_2 feed-forward compensation scheme such as presented in [9]. Since it is necessary to separate the geometric and hysteretic from the dynamic properties to understand the effects in the Tevatron, this note provides detailed discussions of the various b_2 contributions as derived from measurements on several Tevatron dipole magnets as well as on the basis of archive data and calculations. The archive data are the magnetic measurement data recorded on all Tevatron magnets after production and prior to installation. These data can be used to predict the average magnetic field properties of all magnets installed. The archive data do not contain information about the dynamic effects since these effects were not recognized at the time of their recording (in fact the data are negatively affected by them).

1.5) Dynamic Effects in Superconducting Magnets – General Introduction

The recently published PhD thesis by M. Haverkamp, [10], explains the dynamic effects observed in superconducting magnets with current redistribution between the strands in the multi-stranded Rutherford cables from which the magnets are wound. Magnet ends in particular are sources of current redistribution because of the spatially varying dB/dt appearing during the ramp. The current redistribution among strands is not necessarily toward a more balanced one. It is affected by the splice to strand resistances and the complex network of strand-to-strand resistances within the cable. The current redistribution often occurs slowly, with time constants of thousands of seconds, because the currents are running for the most part in zero resistance superconductor. Fast, short time constant contributions, have also been observed. These current imbalances have also been called Boundary Induced Coupling Currents (BICC) [11].

Current imbalances produce local magnetic field variations within the coils, which have a period given by the cable twist pitch. The current imbalances also produce field variations within the magnet bore, the so-called periodic pattern in all (geometrically allowed) field components of the bore field. The periodic pattern is mostly the direct effect of the current imbalance as computed with the Biot-Savart law. The time variation of the magnetic field in the coils as a result of the time variation of the current imbalances also produces a change in the magnetization response of the superconductor. The magnetization response is non-linear, as can be understood on the basis of the

magnetization hysteresis of the single strand. A small negative field change (in one twist-pitch for instance) produces a much larger magnetization change (switch to "other" branch of hysteresis curve) than a positive field change (in the next twist pitch). Therefore the magnetization response is mostly a demagnetization caused by the negative field change. As pointed out by Haverkamp, [10], the dynamic effects are 3D effects because the twist pitch is comparable to the bore size. In this case the dynamic effect in one slice of the magnet is generated not only by the coil (and current distribution) within this slice but also by an upstream and downstream coil section, with diminishing impact with distance. This 3D effect is strongly reducing the amplitude of the dynamic effects and the pattern. Another factor is the twist pitch phase relation between all the turns in the coils. Haverkamp finds that the largest pattern amplitude is produced by the cases in which there is a random phase variation between turns. This is probably related to "destructive" interference between different blocks in the coil cross-section.

The drift effects found in the magnetic multipoles are a direct consequence of the local field variations seen by the strands as a result of the slowly changing current imbalances. During ramping of the magnet these field variations do not affect the cross-sectional multipole distribution because the local field change on the ramp is much larger than that caused by the current redistribution. At constant excitation, however, the hysteretic nature of the magnetization of the strands together with the time varying current redistribution within the cable produce the dynamic behavior of the cross-sectional multipole pattern that can be seen in e.g. Figure 2 and according to the mechanism described above. Following a drift at constant magnet excitation is a so-called snapback at the start of the ramp. During the snapback the demagnetized coil regions causing the multipole drift are being re-magnetized until the local field change of the ramp completely overcomes the local field changes due to the current redistribution.

Decay (and snapback) appears in all allowed (and sometimes also in non-allowed) multipoles and is always directed toward a reduction of the magnetization contribution. Although very short diffusion time constants have been observed, the strongest effects appear to be related to current diffusion time constants of *1000 secs* or more. Drift and snapback amplitudes are approximately equal and uniform along the magnet body. The amplitude of the periodic pattern can vary along the magnet and certainly changes in the magnet ends. The powering (or ramping) history influences the magnitude of the dynamic effects through its effect on the current distribution. The dynamic effects are stronger, the larger the superconductor magnetization.

1.6) Tevatron Dipole Magnet Study Program

Fermilab's Technical Division recently launched a magnetic measurement program to address the issue of tune and coupling drift in the Tevatron and to improve the Tevatron b_2 compensation scheme. Some of the main results of this program will be discussed in this note. Table 2 gives the list of magnets that have been included in the measurement program. Almost all magnets listed are from the Tevatron spare magnet pool. To assess the magnet-to-magnet variation of the dynamic effects the attempt was made to include

Table 2: Characteristics of harmonics study candidate dipole magnets.

	quench perform			quench type		a1 hysteresis	
magnet	low	ave	high	not B	B	<0.1 u	> 0.1 u
TC 0483	×			×			×
TB 0834		×		×			×
TB 0269	×				×	×	
TC 1220			×	×		×	
TC 1052		×		N/A			×
TB 1055		×		N/A		×	
TC 0401	×				×	×	
TC 0525		×			N/A		×
TC 0710		N/A			N/A	×	
TB 1198	×				×	×	
TB 1077		×		×			×
TC 1130			×	×			×
TC 0604			×	×		×	
TB0413		×		×			×

magnets with very different characteristics. Table 2 also lists some general properties of the magnets, such as a rough classification of their quench performance, of their ramp rate behavior (type B or not), whether they show a_1 hysteresis or not and the cable from which their coils are wound. The type B behavior refers to the quench current dependence on the ramp rate. Type B magnets show no significant ramp rate dependence until above a threshold the quench current drops sharply with increasing ramp rate. The table also indicates differences regarding the performance of the cable used in the coils. It is important to note that the superconducting strand used in the cables for the Tevatron magnets evolved throughout the magnet production, resulting in significant increase in the critical current density of strands from the early and last (so called hi-ho) period of strand manufacturing. All magnets listed in the table were measured on the Tevatron test bench at the Magnet Test Facility (MTF).

1.7) Magnetic Measurement Systems

The Tevatron magnets were tested on one of the two remaining horizontal Tevatron type magnet test benches at Fermilab's Magnet Test Facility (MTF), referred to as stands 2 and 6. The Tevatron test benches are fully equipped with feed- and return-cryo-boxes to regulate the flow of liquid helium from the MTF helium liquefier through the magnet. Special *5 kA* power supplies provide the current to the magnet. The test stand is also equipped with an automatic quench protection system, consisting of quench detection circuitry and quench heater power supplies. Temperature regulation is performed via the JT valve in the return box and the pressure regulation in the single-phase pre-cooler. The test stands can be run in the low and high-pressure modes. The latter is the mode in which the magnets are cooled in the Tevatron. Extensive temperature and pressure diagnostics are also included. The magnetic measurements were performed using two different measurement systems: a rotating coil system, specially adapted for the use in

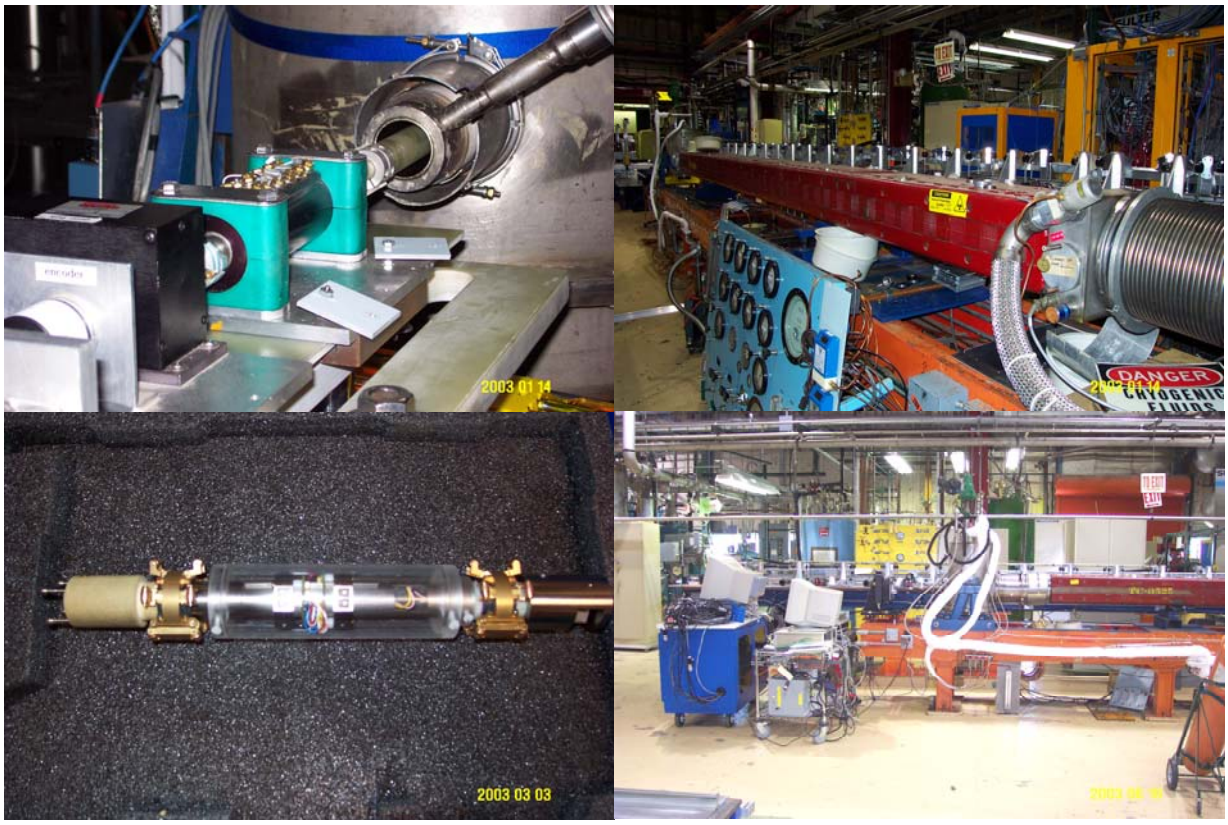

Figure 4: Pictures from the magnetic measurement systems at MTF. Upper left: rotating coil drive system (step motor, gear box, encoder, slipper) and rotating coil system entering Tevatron magnet warm bore, Lower left: Hall probe sextupole array as provided by CERN. Upper and lower right: Tevatron dipole magnet on the test stand 2 at MTF.

Tevatron magnets and a Hall probe array for the measurement of the dipole/sextupole components developed at CERN [12]. Both systems are inserted into a warm-bore mounted into the bore of the magnet. In some instances the two measurement systems were used simultaneously, introduced into the magnet bore each from a separate end. Figure 4 shows some snapshots of both systems as well as the Tevatron magnet test-stand 2 at MTF. The following describes in detail both magnetic measurement systems.

The multipole de-composition of the magnetic field used in the analysis of the magnetic measurement data presented in this report is given in Equ. 1, where the reference radius (r_{ref}) typically used for Tevatron magnets is *25.4 mm*.

$$B_y + iB_x = B_0 10^{-4} \sum_{n=0}^{\infty} (b_n + ia_n) \left(\frac{x+iy}{r_{ref}} \right)^n \tag{1}$$

1.7.1 Rotating Coil Measurement System

The horizontal drive rotating coil system (see Figure 4) is placed inside a warm-bore anti-cryostat inserted into the magnet bore. A *1.8 m* long drive shaft (this is the typical length, other shaft configurations were also used), assembled from G10 rods, is used to transfer the rotation to the probe placed inside the magnet. The shaft is supported with two or three spring-loaded bearings within the warm bore. Figure 5 shows the typical probe positions for body and end measurements used in this study. The body position was chosen such as to require as little shaft length as possible. The system is rotated using a variable speed DC-motor and a 1:8 gear-reducer. The rotating coil probe consists of a *81.7 cm* long coil array wound on a precision machined G10 former at a *19.6 mm* radius. The windings consist of a tangential winding for the measurement of higher order harmonics as well as two dipole coils rotated against each other by *~60* degrees. The signals are transferred from the rotating probe with slip rings. An angular encoder supplies a trigger pulse every 64th part of a rotation.

Coil windings are read out by precision digital integrators, PDI (Metrolab's 5035), which were configured to read and store data in their internal buffer (during the "active" time) and to transfer them to the VME computer (during the "passive" time). The typical system duty factor was 50%. To achieve good temporal resolution the shaft rotational speed was set to *~5 Hz*. To decrease the effect of mechanical vibration and to increase the signal to noise ratio an analog bucking technique was used, providing a cancellation of the main dipole field term with a simple addition of signals from the tangential and dipole coils. Bucking ratios of *~150* are typical. The PDI are triggered with the angular encoder pulse. The PDI module continuously integrates the voltage over time and sends the instantaneous integrated voltage at every encoder pulse to the internal buffer. The internal buffer is transferred after every 2nd rotation to the VME computer. There is no data recording during this transfer for one full rotation. The data from two rotations are then averaged over three rotations. In addition there are corrections for the integrator drift. The data are then digitized, amplified by a set gain (*~50-100* for the bucked

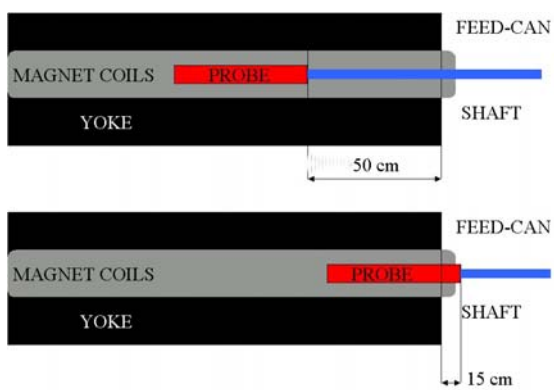

Figure 5: Position of the rotating coil system within the magnet entering from the lead (feed-can) end. Top: body-position, bottom: end position. The total probe length is ~84 cm. The probe position is given with respect to the edge of the iron yoke. As can be seen in the schematic, the coils are extending beyond the iron yoke. Not shown in the plot is the feed-can at the end of the magnet, which typically requires an additional shaft length of ~1.5 m.

tangential coil signal) and bucked against the dipole signal. The digital bucking serves to remove the residual dipole signal remaining after the analog bucking.

The time-integrated voltage induced in the tangential coil as it explores the radial field components around the perimeter is proportional to the magnetic flux in the magnet bore. The integrated voltage (or flux) versus angle (or encoder pulse number) can be described by a superposition of sinusoidal waveforms, with frequencies corresponding to the $n+1^{th}$ multiple of the probe rotational period, where n is the magnetic multipole harmonic number ($n=0$..dipole,..). A Fourier decomposition of this (bucked) signal reveals the amplitudes of the magnetic multipoles. The nth multipole is the amplitude of the Fourier peak at $2\pi/(n+1)$. The total magnetic field in the bore can be reconstructed from the multipole decomposition with the harmonic multipole expansion of the Cartesian field components given in (1). In particular (1) is used to rescale the measurements, which are performed with a tangential coil that is not placed at the reference radius, to the reference radius condition. In the magnet ends the field decreases. It is customary to normalize the end-multipoles to the body field. In this case it is necessary to multiply the multipoles obtained with the ratio of the "average" dipole field measured in the end position divided by the dipole field measured in the body position. Also note that expansion (1) is only valid for the length-integrated fields in the case of the magnet ends.

To account for the possibility that the coil is placed off-center within the magnet bore, a centering correction of the data is performed. The centering correction procedure takes advantage of the large 18-pole ($n=8$) of ~-12.5 units of the Tevatron dipoles. Assuming that any 16-pole ($n=7$, non-allowed) is entirely the result of feed-down from the 18 pole the de-centering correction consists in calculating the Δx and Δy needed to produce the observed 16-pole by feed-down using equation (2). In fact the calculation also includes second order feed-down term to the 14-pole. The a_n,b_n data are then corrected by performing a coordinate system translation in (1) by Δx and Δy. The coordinate transformation consists in substituting the complex position vector z with $z+\Delta z$ and redefining the a_n,b_n such as to reestablish equation (1) in its centered form. A Δz dependent factor gets absorbed into the new "centered" multipoles a_n,b_n.

$$b_7 = 8b_8 \frac{\Delta x}{r_0} \qquad a_7 = 8b_8 \frac{\Delta y}{r_0} \qquad b_8 = -12.5u \tag{2}$$

Other possible systematic measurements errors, for instance due of eccentric rotation of the probe, are not considered to have any impact on the measurements. This and other similar issues were recently investigated for the case of the LHC interaction region quadrupoles [13].

The magnet current is monitored with a DCCT device delivering a voltage proportional to the magnet current to a DVM. The magnet current measurement is not synchronized with the magnetic measurements. In some instances difference of up to *250 msec* were found between them. This needs to be taken into account when plotting the main field versus current to derive, for instance, B_0 hysteresis or B_0 snapback.

1.7.2 Hall Probe Measurement System

The Hall probe sensor used in the experiments reported here is an exact copy of a system used at CERN for the LHC magnet measurement program. A detailed description of the hardware is given in [12], [14]. The Hall array operates at a bandwidth of *10 Hz*, approximately ten times faster than the effective measurement rate of the rotating coil system. It is therefore preferred for the measurement of the fast snapback. Also, the Hall array measures the sextupole locally, making it the preferred choice for pattern measurements (a special sliding fixture was made at CERN that allows fast z-scans for pattern measurements). The sextupole probe (see Figure 4) is built from two rings spaced longitudinally by *~1.25"*[1]. Each ring contains three Hall plates, mounted on the probe support, such as to sample the radial field at three positions located on a circle of radius *14.3 mm* and equally spaced in angle. The probe is oriented so that the Hall plates are placed at *90 degrees*, *210 degrees* and *330 degrees*, measured from the horizontal. Therefore, assuming ideal geometry, the probe array is sensitive only to the sextupole component of the field (and the higher harmonics of the sextupole such as the dodecapole and the 18-pole).

The array consists of two rings spaced by approximately half the twist pitch of the Tevatron dipole magnet cable[1], in order to allow averaging over the longitudinal pattern. This pattern has a longitudinal period equal to the twist pitch of the cable from which the coils are wound. The signal recorded is the sum of the voltages produced by both rings, which, given their spacing by one half of the pattern period, should remove any effect resulting from the longitudinal pattern (unless the pattern is strongly non uniform along z). The signal from the three Hall plates on each ring is amplified with a variable gain amplifier (*G~3.7*) and sent to an adder (*G=20*). In the stage where the two ring signals are added, another amplification (gain *~3*) is applied. The total amplification of the sextupole signal is therefore *~240*. In addition the DAQ software multiplies the sextupole data by an additional factor *10*. The signal from one Hall probe (the one on top) is brought out separately without amplification. With the right orientation (in fact the probe is oriented such as to maximize the signal of this sensor) of the probe, this signal is proportional to the dipole (*1T~1V*) and can be used subsequently to remove the residual dipole from the sextupole signal.

The data reduction procedure for the sextupole, b_2, measured with the Hall plate sensor is given with (3)

$$b_2 = 10^4 \frac{K_2\left(V_2 - V_{offset} - K_{bucking}V_0 - K_{nonlinear}V_0^2\right)}{K_0 V_0} \quad units\ @\ 25.4\ mm, \tag{3}$$

where K_2 is the calibration constant for the sextupole sum signal (sum of ring 1 and ring 2), V_2 is the sum signal, V_{offset} is the offset on the sum signal, $K_{bucking}$ is the residual dipole bucking constant, $K_{nonlinear}$ is the non linear residual dipole bucking constant and V_0 is the

[1] Note that the twist pitch was not held constant in the Tevatron cable production, but rather varied such as to achieve the specified cable thickness and width.

voltage from the dipole probe. V_0 is the signal from the dipole probe. K_0 is the calibration constant for the dipole signal. The correction factor for non-linearity, $K_{non\text{-}lin}$, is usually small and only important when the Hall data are to be used in a wider range of fields.

Many issues, such as variations (e.g. due to temperature) of the sensitivity of Hall plates from nominal, effect of higher order harmonics (such as the strong 18-pole present in the Tevatron dipole magnets), amplifier gains in the analog conditioner and imperfect geometry of the Hall probe array, make it difficult to predict the calibration constants to a accuracy better than a few %. Therefore it is necessary to calibrate the Hall probe results on rotating coil measurements. This procedure automatically implies that the Hall-probe multipole data refer to the same reference radius as the rotating coil data. Strictly speaking, the calibration factors K (which are related to the Hall probe sensitivities (V/T) and the geometry), the sensor offset V_{offset} are found from a comparison of a part of the hysteretic loop (preferably close to the snapback region) as recorded by Hall probes and rotating coils. Table 3 lists typical calibration parameters. Further details regarding this procedure can be found elsewhere [12].

Table 3: The conversion constants typically used for the dipole and sextupole conversions for the sextupole measurements on Tevatron dipole magnets using Hall probes.

	V_{offset} (V)	K_n (T @ 25.4 mm / V)	$K_{bucking}$ (-)	$K_{non\text{-}linaer}$ (1/V)
dipole	0	0.92674	0	0
sextupole	0.18615	-0.0095	-0.30539	-0.0967

1.8) Magnetic Measurement Procedure and Current Cycle

The current cycle used in this Tevatron dipole measurement campaign is (almost) identical to that of the accelerator operation. It is shown together with the naming convention for the various porches in Figure 6. The exact current ramp settings are listed in appendix 1. The magnets are quenched at high current before each measurement cycle to raise the coil temperature above critical and to erase all BICCs (and thus to erase the effect of the previous ramping history on future drift measurements). The nominal magnet current/field at injection level is *666 A* (*~0.660 T*), and *4333 A* (*~4.330 T*) at flat-top level. The ramp-rate during the linear acceleration ramp is *~50-70 A/s*, and a full swing (from injection to flat-top) takes about *80 sec*. Acceleration starts with a parabolic time dependence before reaching full speed. The original purpose of the back-porch was to extract anti-protons from the Tevatron, while the excursion to the lower energy reset point is needed in order to locate the injection point on the up-ramp of the hysteretic b_2 loop. We will refer to the different porches by their abbreviations in the following: FP, FT, BP and IP stand for pre-cycle front-porch, pre-cycle flat-top, pre-cycle back-porch and injection porch. FTE and NFT stand for flat-top energy and number of flat-tops.

The measurement program was designed to explore the dynamic effects in Tevatron dipoles following the so-called standard pre-cycle. The standard beam-less pre-cycle in

the Tevatron today consists of a "dry-squeeze", that is a *~20 min* FT, followed by a *~1 min* BP. Some of the pre-cycle parameters were varied, however, as listed in Table 4. The protocol consisted in varying the pre-cycle FP, FT, BP and IP durations to simulate the effect of powering history on the dynamic effects. In addition, the FTE and the NFT was varied (the variation of the FTE, however, has no impact on Tevatron operations, since the maximum current is now always held at *4.33 kA*). A full program was usually completed for each of two probe positions, i.e. in the body and the end of the magnet (see Figure 5 for the exact probe positions). Also, the full set of measurements was usually repeated at a different temperature. The standard measurement temperature was *~4.0 K*. The lowest temperature point was usually *~3.8 K*, the highest *4.4 K*.

While powering Tevatron dipole magnets at MTF with a typical Tevatron ramp a current overshoot of up to *2 A* was observed at the end of the ramp to the injection plateau, which is approached at a high ramp-rate according to the current Tevatron ramping protocol (~ *70 A/s*). This overshoot is considered excessive for quality magnetic measurements, and raised doubts that MTF power supplies were able to accurately reproduce Tevatron current ramps, where current overshoots are not observed. A simple feed-forward approach was chosen to eliminate the overshoot, by slightly modifying the power supply drive signal during the approach of the injection porch. The modified ramp profile and the resulting current profile are shown in Figure 7. The overshoot has been completely eliminated for the first measurements of TC1220, and the current closely follows the intended profile. Applying this simple recipe to other magnets and cases (for example measurements with MTF test-stand 6) we observed that the current overshoot substantially decreased and didn't exceed 0.25 A. In some cases, however, a stronger over-shoot re-appeared despite of the correction.

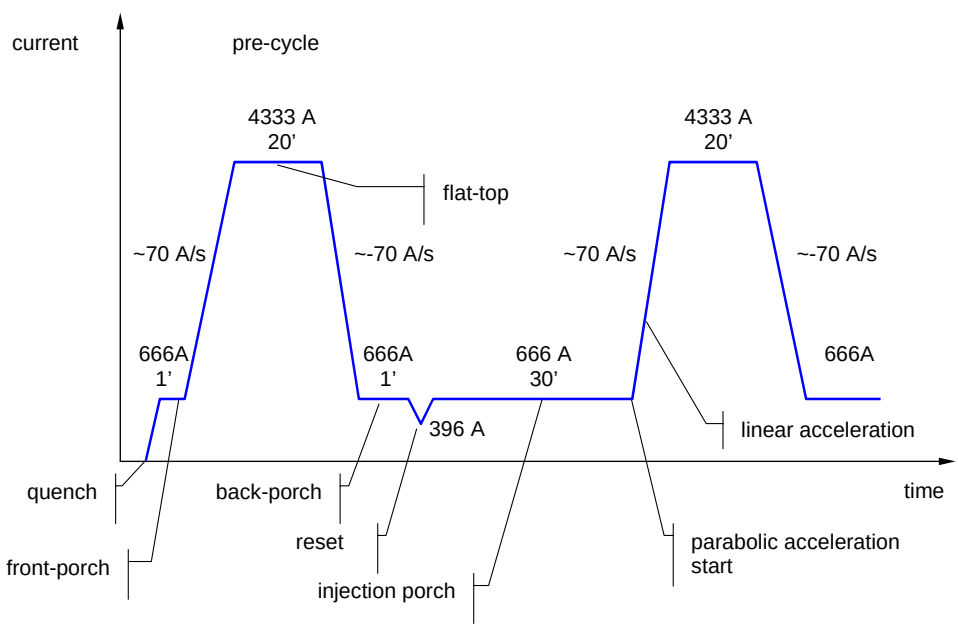

Figure 6: Standard current cycle for the Tevatron dipole magnetic measurements including nomenclature.

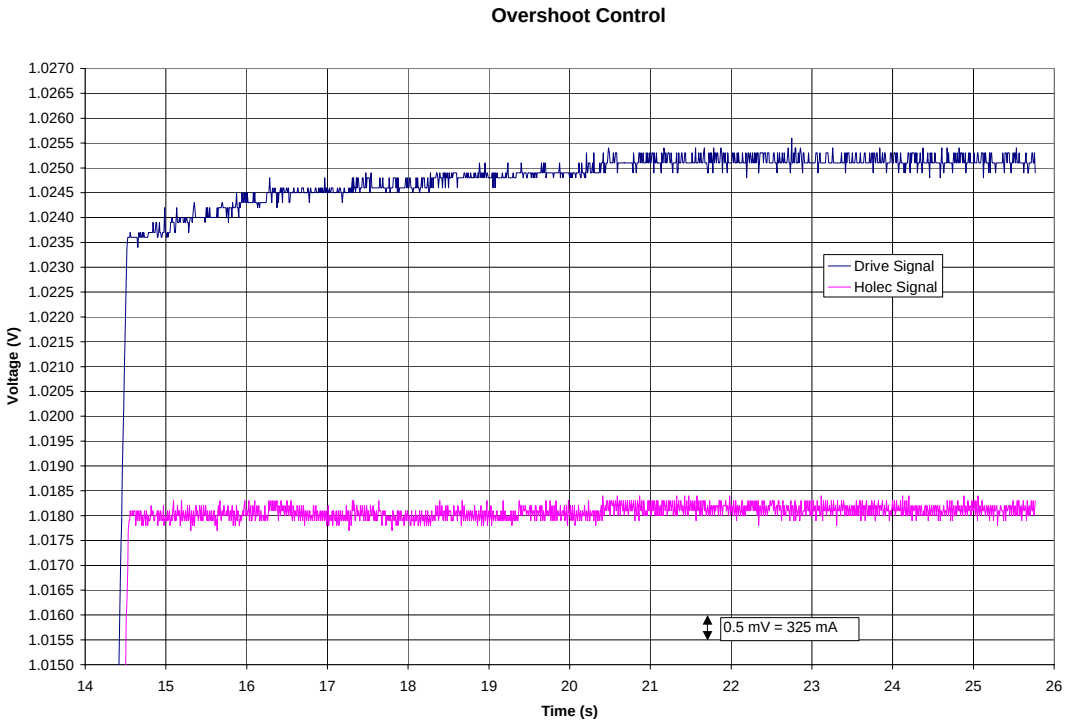

Figure 7: Overshoot-free current profile in magnet approaching the injection porch (below) by modifying the drive signal (top).

In order to formulate a multi-parameter fit for the b_2 drift and snapback, measurements in which the parameters are varied in a wider range (especially in the case of the back-porch and flat-top durations) are necessary. The results of the dynamic effect measurements using variable wave-form parameters will be discussed further in chapter 4. Table 4 contains the internal numbering scheme for the various types of powering waveforms that were used. Originally the parameters were varied on the basis of a "standard" pre-cycle (1 min front-porch, 20 min flat-top, 1 min back-porch and 30 min injection-porch). One of the results of this measurement campaign was the suggestion of a new pre-cycle with a 60 min flat-top and a 5 min back- porch. Therefore the numbering scheme was changed mid-way through the measurement campaign. The new numbering scheme used the durations of the front-porch, flat-top, back-porch and injection porch durations (in mins) as the measurement number (when the durations were secs a "s" was added after the value given to the respective porch). Table 4 does not take into account all types of measurements that were conducted. Variations of bath temperature or ramp-rate, for instance are not mentioned.

Table 4: Measurement program for Tevatron magnets. The standard cycle (# 7,12,16) has the following parameters: 1 pre-cycle with 20 min FT, 1 min BP, 30 min IP, FTE 980 GeV. Each measurement was preceded by a quench. The number in the left column is an internal identifier. A new numbering scheme was introduced halfway through the measurement program. It consisted in explicitly stating the durations of the various porches.

#	parameter	value	fixed parameters
7	BP	1 min	1 min FP, 20 min FT, 30 min IP
01200330	BP	3 min	1 min FP, 20 min FT, 30 min IP
01200530	BP	5 min	1 min FP, 20 min FT, 30 min IP
8	BP	10 min	1 min FP, 20 min FT, 30 min IP
01201530	BP	15 min	1 min FP, 20 min FT, 30 min IP
9	BP	30 min	1 min FP, 20 min FT, 30 min IP
10	FT	1 min	1 min FP, 1 min BP, 30 min IP
11	FT	10 min	1 min FP, 1 min BP, 30 min IP
12	FT	20 min	1 min FP, 1 min BP, 30 min IP
13	FT	60 min	1 min FP, 1 min BP, 30 min IP
51	FT	60 min	1 min FP, 1 min BP, 30 min IP
52	FT	120 min	1 min FP, 1 min BP, 30 min IP
53	FT	360 min	1 min FP, 1 min BP, 30 min IP
54	FT	720 min	1 min FP, 1 min BP, 30 min IP
01010530	FT	1 min	1 min FP, 5 min BP, 30 min IP
01100530	FT	10 min	1 min FP, 5 min BP, 30 min IP
01200530	FT	20 min	1 min FP, 5 min BP, 30 min IP
01600530	FT	60 min	1 min FP, 5 min BP, 30 min IP
011200530	FT	120 min	1 min FP, 5 min BP, 30 min IP
012400530	FT	240 min	1 min FP, 5 min BP, 30 min IP
14	FTE	800 GeV	1 min FP, 20 min FT, 1 min BP, 30 min IP
15	FTE	900 GeV	1 min FP, 20 min FT, 1 min BP, 30 min IP
16	FTE	980 GeV	1 min FP, 20 min FT, 1 min BP, 30 min IP
7	NFT	1	1 min FP, 20 min FT, 1 min BP, 30 min IP
17	NFT	2	1 min FP, 20 min FT, 1 min BP, 30 min IP
18	NFT	3	1 min FP, 20 min FT, 1 min BP, 30 min IP
19	NFT	6	1 min FP, 20 min FT, 1 min BP, 30 min IP
6fastpc	NFT	6	1 min FP, 1 min FT, 1 min BP, 30 min IP
7	IP	30	1 min FP, 20 min flat-top, 1 min BP
6	IP	60	1 min FP, 20 min flat-top, 1 min BP
5	IP	120	1 min FP, 20 min flat-top, 1 min BP
4	IP	240	1 min FP, 20 min flat-top, 1 min BP
01200530	IP	30	1 min FP, 20 min flat-top, 5 min BP
01200560	IP	60	1 min FP, 20 min flat-top, 5 min BP
012005120	IP	120	1 min FP, 20 min flat-top, 5 min BP
012005240	IP	240	1 min FP, 20 min flat-top, 5 min BP
01200130	FP	1	20 min FT, 1 min BP, 30 min IP
05200130	FP	5	20 min FT, 1 min BP, 30 min IP
30200130	FP	30	20 min FT, 1 min BP, 30 min IP
01200103s	IP	3 sec	1 min FP, 60 min FT, 5 min BP
01200106s	IP	6 sec	1 min FP, 60 min FT, 5 min BP
01200112s	IP	12 sec	1 min FP, 60 min FT, 5 min BP
05200120s	IP	20 sec	1 min FP, 60 min FT, 5 min BP
30200130s	IP	30 sec	1 min FP, 60 min FT, 5 min BP
0110s06s06s	IP	6 sec	1 min FP, 10 sec FT, 6 sec BP

2) Geometric b2

A particularity of the Tevatron dipole magnet design is that the geometric b_2 component is relatively large (order *0.1%* or *~14* units) everywhere in the straight section. This positive b_2 is needed to compensate for the strong negative b_2 spike of *~-600* units in the ends, the result of a simple, compact end-design. The body and end b_2 usually integrate to zero. The following summarizes our knowledge on the geometric b_2 in Tevatron dipoles on the basis of calculations, archive data of the pre-installation magnetic measurements as well as recent magnetic measurements.

2.1) Tevatron Magnetic Measurement Archive Data

All Tevatron dipole magnets produced were tested at Fermilab's MTF prior to installation in the Tevatron. The tests also included extensive magnetic measurements of the field quality, field integral (transfer function) and field angle. A database contains the results of all magnetic measurements taken with rotating coils for *0-4kA-0* current loops. These data can be used to derive the b_2 of any Tevatron dipole magnet as well as the total average b_2 in the entire ring. The geometric b_2 was derived from the "up-down" average of the hysteretic loop b_2 at *2 kA*. Assuming that the hysteretic loop is symmetric around the geometric multipole, this procedure generates the sought geometric multipole. Figure 8 shows the histograms of the "body-end combined" up-down average b_2 at *2 kA* data. The combined b_2 averaged over all Tevatron dipoles currently installed in the Tevatron obtained according to this procedure is *~1.47 units*. Table 5 summarizes the archive b_2 data, showing a difference between the b_2 in the ends (*~-7 units*) and body (*+14.4 units*). Note that the data given in Table 5 were taken with *~2.4 m* long probes. In the end position these probes were therefore measuring not only the strong negative b_2 excursion but also a substantial positive b_2 from the straight section segment covered by the probe. The combined data represent the overall average of the b_2 over the entire length of the magnet. Ideally the combined b_2 should be zero.

Unfortunately the average b_2 hysteresis loop of the Tevatron dipoles (see section 3) is not symmetric around the geometric, with some high current effects distorting the loop downwards. Furthermore, the drift effects were unknown in the 1980s and inadvertently affected the measurements summarized in the above table. The magnetic measurements were performed at a fixed current to allow for measurement-coil winding and un-winding (the magnetic measurement was performed during the un-wind). During this time the b_2 was drifting. Therefore the up-down averages for the three different positions, downstream and upstream ends as well as center, in Table 5 are not exactly the geometric b_2*s* to which the Tevatron tends at high current. Figure 9 shows the average b_2 in the Tevatron at *4 kA (~900 GeV)*, also derived from the body-end combined archive data. This value is *0.83* units, which under-estimates the all Tevatron average geometric b_2. This value, however, can be used to reconstruct the average high current geometric b_2 in the Tevatron. To the all Tevatron average b_2 at *~4 kA* of *~0.83 units* we add *0.4 units*, which is the average half-width of the hysteretic loop at the same current of all the

Table 5: Mean and sigma of up-down averages of b_2 (in units of 10^{-4} of the main dipole) at 2 kA in all Tevatron dipoles currently installed in the ring in up-stream end, down-stream end and body position (center) as well as combined data.

	Combined		Downstream		Upstream		Body	
	Ave	σ	Ave	σ	Ave	σ	Ave	σ
b_2	1.47	3.09	-6.79	3.22	-6.92	3.2	14.39	3.08

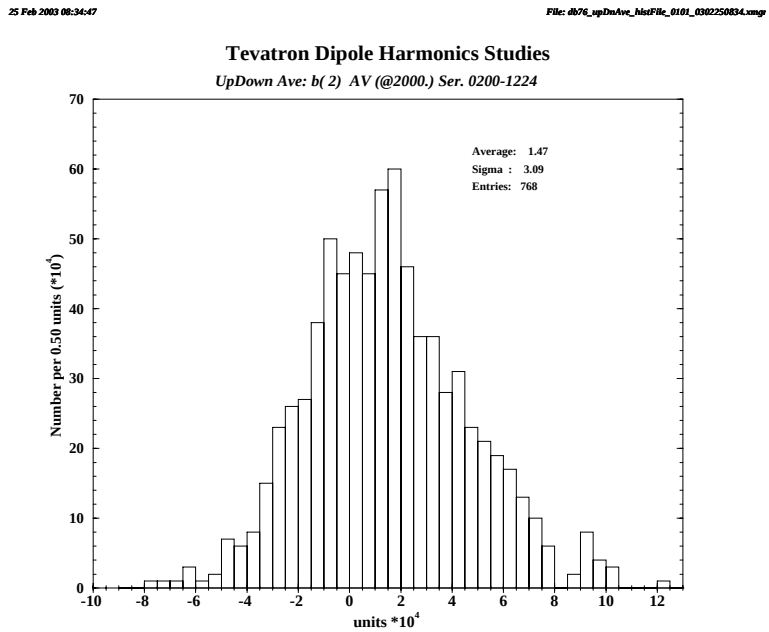

Figure 8: Tevatron dipole archival magnetic measurement data: Average geometric b_2 (in units at 25.4 mm) of all Tevatron dipoles installed, as calculated from the up-down average at 2 kA (up-down referring to the measurements performed during the up and down ramps).

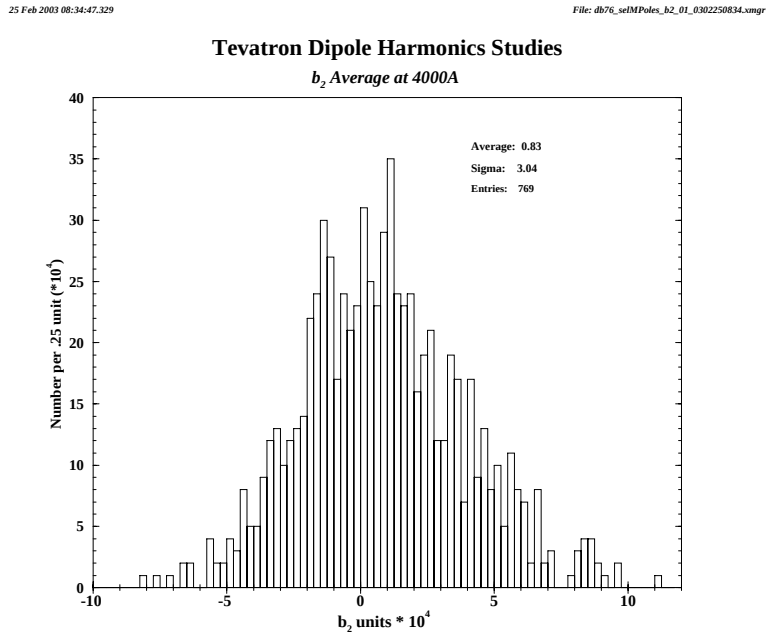

Figure 9: Tevatron dipole archival magnetic measurement data: Average b_2 (in units at 25.4 mm) of all Tevatron dipoles installed at 4 kA (~900 GeV beam energy).

recently measured magnets (more on the hysteretic b_2 in section 3). This gives *1.23 units*, which is a little less than the *1.47* units obtained on the basis of the up-down branch average of all Tevatron dipoles at *2 kA* (this derivation is discussed further in [9]).

2.2) Magnetic Models of the Tevatron Dipole

More details on the magnetic field simulations of Tevatron dipoles can be found in [15]. Analytical, numerical (ROXIE[2]) and finite element (OPERA[3]) models of the Tevatron dipole magnets were generated. These models reproduce the multipole content of the average Tevatron dipole magnet as derived from the magnetic measurement archive (see Table 6).

Table 6: Multipoles (in units of 10^{-4} of the main dipole) in straight section and end of Tevatron dipoles, calculated with ROXIE 9.0 and average calculated from archive data. The current at injection is 666 A. The multipole index n is according to the US notation (corresponding to the 2n+2 pole). The calculated multipolar field components in the ends were averaged over a 50 cm end section. The end multipoles quoted are given in units of 10^{-4} of the straight section dipole.

n	0 (T)	1	2	3	4	5	6	7	8	9	10
calc body	0.6658	0	12.9	0	2.2	0	4.4	0	-12.3	0	4.2
archive body	0.6658	0	14.4	0	1.83	0	5.28	0	-12.5	0	3.8
calc end	0.5786	0	-78	0	-12.7	0	1.4	0	-10.5	0	2.9

Once calibrated on the average multipole content of the Tevatron dipole according to the archive data, the models were used for an analysis of the geometry parameters affecting b_2 (see [15] for further details). The most important parameter affecting b_2 is the pole-angle, which can be regulated via the azimuthal coil pre-stress. The calculated effect of a *1º* variation of pole angle in the inner or outer layer is *20* b_2 *units*. A *0.5º* variation in the inner layer pole-angle corresponds to an azimuthal coil size variation of *0.35 mm*. Another important coil geometry parameter is the mid-plane shim (i.e. the insulation layer underneath the coil in the mid-plane). A variation in inner layer shimming of the order of *0.2º* (or *~150 µm*) generates a b_2-variation of more than *10 units* if the pole-angles remain unchanged and up to *20 units* if the pole-angles change at the same rate as the mid-plane angles. The OPERA models were also used to calculate iron yoke saturation effects, showing that they are of the order of *0.4 units* in b_2 (and entirely negligible in the case of the higher order multipoles).

A 3D magnetic model of the Tevatron dipole ends was generated with ROXIE 9.0. The model calculations were successfully compared to measurements of the end-fields in Tevatron dipole TB1055 using a short probe. In this model the end is (arbitrarily) defined as the *50 cm* long region, which begins *34.5 cm* before the end of the yoke and ends *3.2 cm* after the physical end of the coil. The b_2 goes through a *~-600 unit* spike in

[2] S. Russenschuck, S. Kurz "Numerical Simulation of Superconducting Accelerator Magnets", IEEE Transactions on Applied Superconductivity 12, N. 1, pp. 1442-1447, 2002
[3] Trademark of Vector Fields Limited

the region where the coils bend. The end spikes are compensated with the *~14 units* of positive sextupole in the body. The equivalent magnetic length of the magnet (i.e. the length of the equivalent magnet with a step function magnetic field) is *6.116 m*. The calculated end-multipoles given in Table 6 are averaged over the *50 cm* end region.

2.3) Recent Measurements

Table 7 shows the results of measurements of the geometric b_2 in body and end of the eleven magnets measured recently at MTF. The geometric b_2 is defined as the average of the up and down ramp values of b_2 at *4 kA*. The end b_2 is the average over the *~83 cm* long magnetic probe, which covers not only the end but also a part of straight section. Therefore some of the negative end b_2 is compensated for. The calculated end b_2 in Table 6 was obtained after averaging over a *50 cm* region, therefore including slightly less straight section and giving a more negative b_2 value than those in Table 7. In Table 7 the recently obtained body and end measurement data were also combined using equation 4 below to generate an overall average geometric b_2, for each magnet. Equation 4 assumes that the body b_2 is constant over the entire magnet length that is not covered by the measurement coil in the "end-position". In the end measurement position the measurement coil reaches to *~68 cm* from the end of the yoke (Figure 5).

$$b_2^{ave} = b_2^{body}\frac{2\times 231.5cm}{2\times 314.5cm} + b_2^{end}\frac{2\times 83cm}{2\times 314.5cm} = b_2^{body}0.736 + b_2^{end}0.264 \qquad (4)$$

For comparative purposes Table 7 also contains the geometric b_2 data for the body and end as computed from the Tevatron magnetic measurement archive. Note that these data were derived from the up-down loop averages at *2 kA* and, as discussed above, include drift effects. Only if the amount of drift that occurred before the measurement was similar on the up and down-ramp points this procedure in fact produced the right geometric b_2. In this comparison the recent data are also up-down averages at *2 kA* to exclude the effect of variations of the geometric at high current. In addition, as will be discussed further below, the geometric b_2 varies along the length of the dipoles. The fact that the probes used in the recent campaign were shorter (*83 cm*) than those used in 1980 (*2.4 m*) means that they averaged differently over these variations! Despite the drift effects in the archive data and the effect of the longitudinal b_2 variation, the comparison of the body b_2 shows remarkable agreement, given that two very different measurement systems were used and given that the measurements are spaced by more than *20 years*. Also the body-end averages show remarkable agreement.

Table 7: Recent and 20 year old results of b_2 measurements on several Tevatron dipoles. The geometric b_2 is defined as the average of the up and down ramp values of b_2 at 2 kA. *Measurements were obtained with probes of different lengths and therefore for different levels of end-body cancellation.

magnet	comment	measured in 2002/03			archive data (1980s)		
		body	end*	ave	body	end*	ave
TC 0483	Problem with end measurements	17.6	N/A	N/A	16.9	-4.0	4.2
TB 0834	Problem with end measurements	13.8	N/A	N/A	13.2	-8.7	-0.0
TB 0269		17.3	-35.0	4.4	17.2	-2.8	5.5
TC 1220		6.4	-48.3	-6.7	6.5	-6.5	-6.5
TC 1052		17.8	-35.4	3.7	16.3	-4.8	3.5
TC 1077	End Measurement wasn't performed	13.5	N/A	N/A	12.5	-9.1	-0.5
TB 1055	End Measurement wasn't performed	17.5	N/A	N/A	16.7	-3.9	3.9
TC 0525		8.8	-57.4	-7.8	8.5	12.6	-4.3
TB 1198		15.8	-57.5	-2.0	15.4	-6.0	2.4
TC 0710		13.5	-59.8	-4.3	14.3	10.1	-0.53
TC 0504	End Measurement wasn't performed	13.1	N/A	N/A	10.3	-9.4	-1.6
TB 1130	End Measurement wasn't performed	16.1	N/A	N/A	15.0	-7.1	1.5

2.4) Z-Scan – End Measurements and b2 Variation Along Body

Z-scans of the end fields were performed with a short (~ *4 cm*) rotating coil probe in the lead end of the Tevatron dipole model TB1055. The probe sampled the bore field at a radius of *12.405 mm*. The 3D model of the Tevatron magnet (see description in section 2.2 and in [15]) was calibrated on these measurements. The results of the measurements are shown together with the model calculations in Figure 10. Despite an unexplained longitudinal shift of the model with respect to the experimental data (most likely related to an uncertainty in the probe position during the z-scan measurement), the agreement is sufficiently good. The coil length of the ROXIE model as well as the exact position of the "end-bend" was chosen such as to fit the well-known equivalent magnetic length of the Tevatron dipoles (*6.116 m*). The equivalent magnetic length corresponds to the length in the product of length and straight section bore field that gives the same total length integrated dipole field as measured in the magnet.

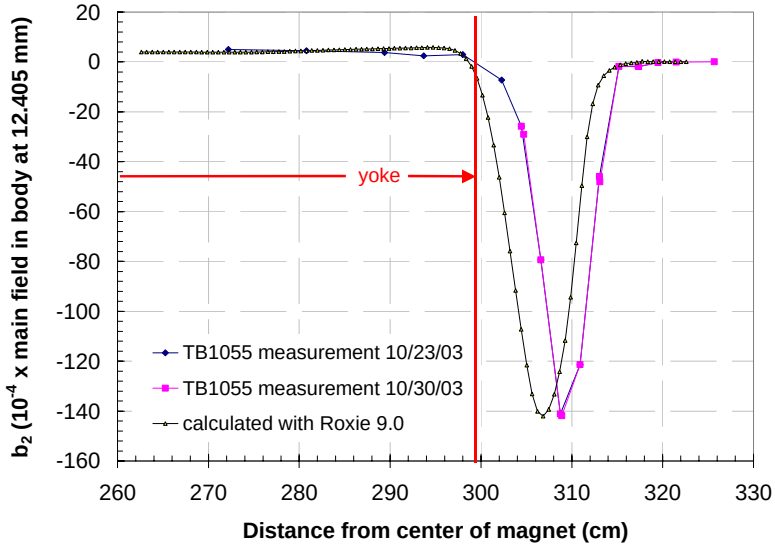

Figure 10: Comparison of ROXIE 9.0 model with z-scan rotating coil measurement in magnet TB1055. Shown is the b_2 multipole along the end at the measurement radius of 12.405 mm. The ROXIE-model was fine tuned to agree with the experimental data. The discrepancy of the position of the b_2 spike is most likely the result of an offset in the position of the measurement system. The coil ends in the ROXIE model were positioned in z such as to produce a dipole field profile, which is consistent with the 6.116 m total magnetic length of the Tevatron magnets.

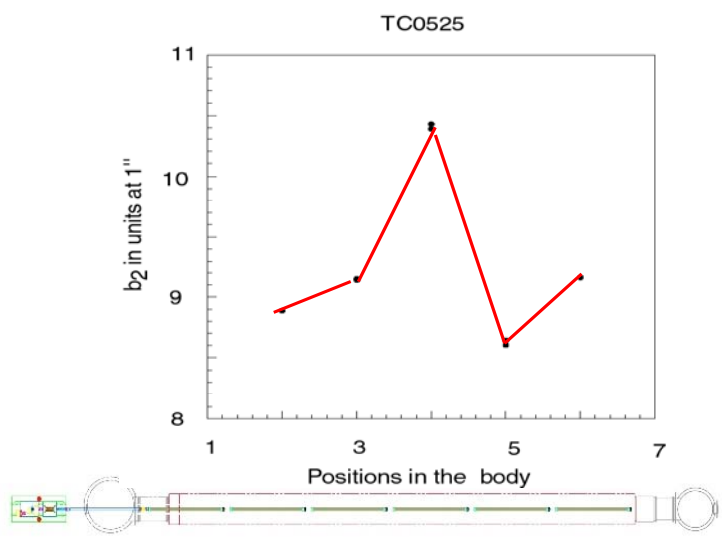

Figure 11: Longitudinal variation of b_2 in TC0525. The schematic below shows the positions of the rotating coil in the magnet.

Figure 11 shows a b_2 z-scan obtained with the *83 cm* rotating coil in the body of the Tevatron dipole TC0525. To check the measurement reproducibility and to verify if the b_2 was stable in time, some points were measured twice (positions 4 & 5), involving a complete disassembly and reassembly of the shaft array. The result in the figure clearly shows a longitudinal variation of b_2 of *~1-2 units*. Note that each measurement point is an average over *~83 cm*, thus an even larger b_2 variation is possible for shorter distances.

Also note that the geometric b_2 quoted in Table 7 is *8.8 units*, i.e. the value obtained in measurement position 2 (which is very close to the standard body position - see Figure 5). The observed b_2 variation is not unexpected and can be explained by longitudinal variations of the pole angle in the inner layer of $0.05°$ (~$35\ \mu m$) or other small coil geometry variations.

2.5) b2 Pattern

The so-called periodic pattern is usually counted as a dynamic effect, since it is the signature of current imbalances in the superconducting cables making up the coils. The periodic pattern is a minute (*0.1 %* level) modulation of the field amplitude, usually affecting all allowed multipoles and decreasing in amplitude the higher the order. In this sense the periodic pattern is a modulation of the geometric field contribution. That is why we chose to discuss it here. The period of the periodic pattern is usually the twist pitch of the inner layer cable. Its peak-to-peak amplitude is typically several units.

It is believed that the periodic pattern is not relevant to the beam dynamics in the accelerator. Note that the pattern adds to the "natural" longitudinal b_2 variation discussed above. It is important, however, to understand the pattern because of its impact on the results of rotating coil measurements. The rotating coil used mostly in the here presented measurements is ~*83 cm* long. The twist pitch of the Tevatron magnet cable and therefore the period of the periodic pattern is ~*2.5"*. The rotating coil therefore averages over ~*13* periods, but, as a result of its length not being an integer multiple of the pattern period there is usually a residue of pattern in the data. Any residual pattern effect, although strongly attenuated, introduces an "error" in e.g. the measurement of the dynamic effects. This effect will be discussed further in chapter 4.

Figure 12 shows the result of the first measurement ever of the periodic pattern in a Tevatron dipole (TB1055). The measurement was obtained during a one-hour dwell on the injection porch (following a so-called standard pre-cycle) with a short (~*4 cm*) probe, that was pulled in steps of ~*1 cm* through a part of the straight section of the magnet. The measurement was not started before ½ hour after the beginning of the injection plateau to minimize the effect of the b_2 drift (which, as will be discussed in chapter 4 is logarithmic in time and thus slowing down considerably after the first few minutes). The pattern data presented in Figure 11 were corrected for an approximately linear (or slightly quadratic) drift of ~*-4 units / 20 cm*. Currently it is believed that this variation is the result of the "natural" variation of b_2 along the magnet (see discussion in 2.4)). Since the total measurement time was comparable to the typical time constant of the current re-distribution (this time constant can be derived from the drift behavior that will be discussed in chapter 4), however, it is to be expected that the pattern amplitude was also changing during the measurement. Therefore this time-dependence has to be added to the expected spatial variation of the pattern amplitude.

Also, the data presented in Figure 11 include a correction for the length of the probe, being similar to the length of the pattern period. The measured b_2 is actually averaged over the probe length and needs to be de-convoluted. The correction factor is given in

equation 5. It depends on the probe (active) length (*4.3 cm*) and the pattern period (which can be inferred from the raw data, here *6.2 cm*).

$$b_{2,pattern} = \left\{ 2\pi \frac{L_{probe}}{L_{pattern}} \left[1 - \cos\left(2\pi \frac{L_{probe}}{L_{pattern}} \right) \right]^{-1} \right\} \times b_{2,raw} = 3.23 \times b_{2,raw} \tag{5}$$

The first pattern measurement presented in Figure 12 reveals a peak-to-peak amplitude in the pattern of *~6 units*. The pattern period is *~6.2 cm* (*2.44"*), very close to the approximate value of the cable twist pitch of *2.5"*. This measurement represents a proof of existence of the pattern. Given the issues mentioned above, the observed amplitude variations could be a result of temporal as well as spatial variations of the pattern amplitude. Also note that the twist pitch was not held constant in the production of Tevatron cables, but rather varied such as to satisfy the specified cable dimensions.

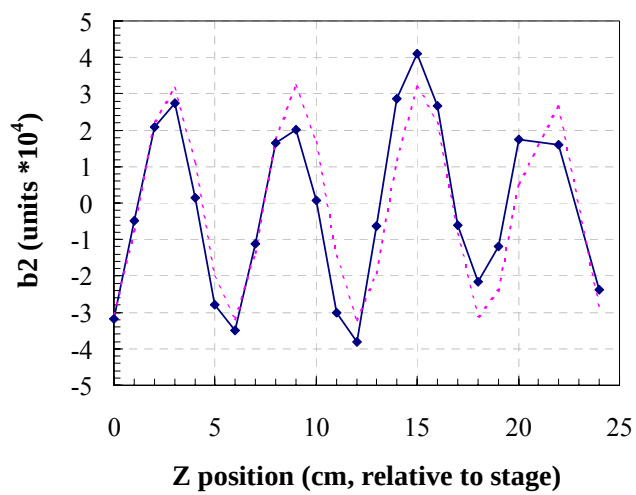

Figure 12: First measurement of b_2 pattern in body of Tevatron dipole TB1055. Dashed-line: cos-function with 6.2 cm wavelength as a guide to the eye.

More systematic studies of the pattern are planned in the future with the CERN Hall-probe array sensor.

3) Hysteretic b2

The hysteretic b_2 behavior in Tevatron dipoles is mostly the result of superconductor magnetization. The hysteretic loop evolves around the geometric b_2, with a loop width proportional to the superconductor magnetization. During ramping of the machine the magnet b_2 usually follows the up-branch of the hysteresis. The magnetization hysteresis is invariant with almost all operational parameters except for the temperature. The following discusses the hysteretic b_2 as derived from the archived production magnetic measurements of all Tevatron dipoles, recent hysteresis measurements in several dipoles as well as model calculations. We will compare recent measurements to the archival data and also discuss body-end differences and the effect of temperature.

3.1) Hysteretic - Archive Data

Figure 13 show the distribution of the hysteretic b_2 widths of all magnets currently installed in the Tevatron at *0.66 kA* (injection) and *2 kA*. These distributions were reconstructed from the Tevatron magnetic measurement archive. It is expected that the archive data underestimate the width because of the drift effects, unknown at the time of the data recording. The histogram indicates a width of *9.45 units* (σ*=1.34 units*) at *0.66 kA*. As expected the loop is narrower at *2 kA*, with a total width of *1.53 units* (and at this current drift effects are less important). On the basis of the data in these figures a hysteretic loop for the average Tevatron magnet could, in principle, be reconstructed. Such a loop is symmetric around the overall average geometric b_2 as given in Table 5 (*1.47 units*) and goes through *1.47-4.73 units* at *0.66 kA* and *1.47-0.77* units at *2 kA*. Note, however, that this loop would be too narrow and underestimates the b_2, especially at injection, because of the drift that occurred in the measurements recorded in the archive. Furthermore the magnetization loop is not necessarily symmetric around the geometric. Also, the archived b_2 loop data include only a few points (*0.66, 2* and *4 kA* on the up and *0.66* and *2 kA* on the down ramp), further complicating the reconstruction. Despite these caveats such a loop was constructed and it is shown in Figure 15.

The recently measured hysteresis loops in several Tevatron dipoles, however, can be used to refine the reconstruction process. First the high current geometric can be found from the all Tevatron average b_2 at *~4 kA* (Table 5) and the average half-width of the hysteretic loop at the same current of all the recently measured magnets (Table 8). These measurements do not suffer from drift effects because they were made "on the fly". This gives *1.23 units* for the high field geometric, which is a little less than the *1.47 units* geometric average of all Tevatron dipoles at *2 kA*. This discrepancy is consistent with the fact that the Tevatron dipole b_2 loops tend to bend downwards at higher current.

Another noteworthy particularity of the histogram in Figure 13 is that it shows two peaks. Indeed, as discussed in [16] the strands used for the Tevatron dipole magnets fall into two very different classes in terms of their magnetization behavior. Although the different types of strands were mixed at the cable/coil level the effect appears also in the magnets.

Table 8: Hysteretic b_2 (units) width at 4 kA in recently measured Tevatron dipoles at 4.0 K.

Dipole	504	483	1198	1052	269	710	1220	1077	525	834	1055	**average**
b2 width 4kA	0.4	0.8	0.8	0.35	0.65	1.2	1.0	0.8	1.0	0.5	0.85	**0.76**

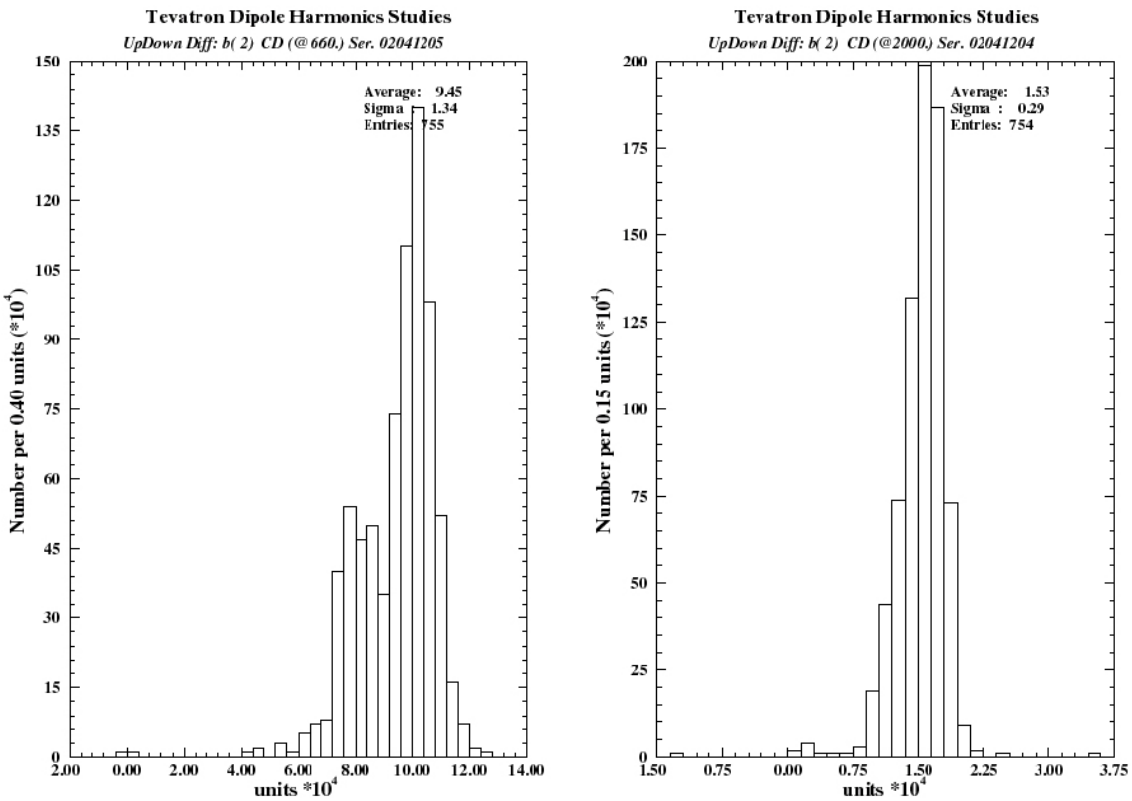

Figure 13: Tevatron dipole archival magnetic measurement data: Left: distribution of b_2 loop widths (in units at 25.4 mm) at 0.66 kA of all Tevatron dipoles installed. Right: distribution of b_2 loop width (in units at 25.4 mm) at 2 kA of all Tevatron dipoles installed.

3.2) Summary – Recently Measured b2 Loops

The invariance of the hysteretic b_2 loop to essentially all operational parameters (except the temperature) makes it a good gauge of the quality of magnetic measurements. Figure 14 shows a compilation of sixteen b_2 loops recorded in the context of the recent measurement campaign in the body of the Tevatron dipole TC 1220. As can be seen the measurement reproducibility is good. Also shown in the figure is a model calculation using the critical current density in the superconductor and the coil and cable / strand geometry. More details on the model calculations can be found in [15].

Figure 15 shows a compilation of b_2 loops measured recently in the body of several spare Tevatron dipole magnets. Most loops were measured at *4 K*, which is close to the average coil temperature in the Tevatron today. In some cases the loops had to be temperature corrected using a linear correction factor (*16%/K* factor - see below in

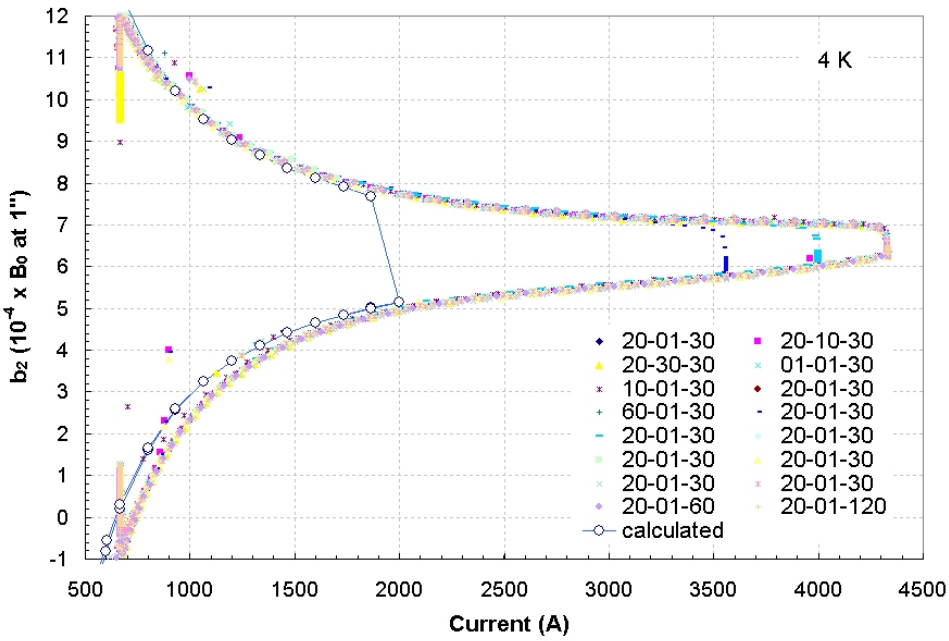

Figure 14: Sixteen different b_2 loop measurements at ~4 K in TC 1220. Labels refer to varying flattop, backporch and injection-porch durations (in min). Also shown is a calculation performed with Maelstrom (courtesy of L. Bottura / CERN). The calculated loop (calculated for zero geometric) was shifted into the measured loops.

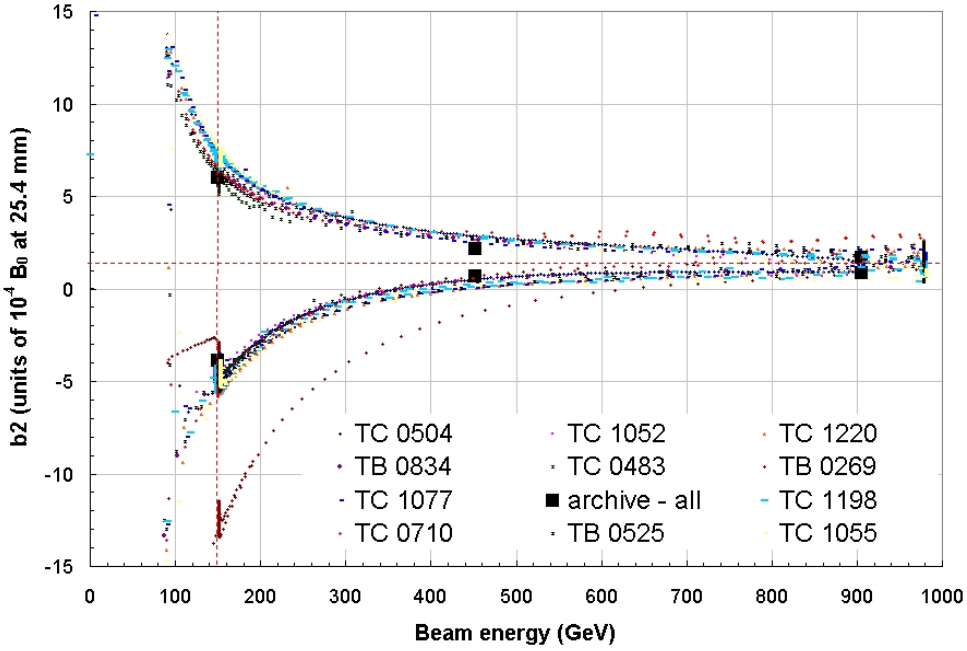

Figure 15: Collection of b_2 loops recorded in the body of eleven magnets recently measured at 4 K. All loops were moved into a geometric of 1.47 units, the average geometric b_2 in the Tevatron according to the archive data (Table 5). Also included is a hysteretic loop reconstructed from the archived hysteretic widths as shown in Figure 13. TB0269 has an unusually shaped hysteretic loop. Some magnets (such as 710) show a yet unexplained, different high current behavior.

section 3.4 for further discussion). The loops were also moved into the average, overall geometric b_2 of the Tevatron (*1.47 units*) as derived from the archive (see Table 5). Also shown in the plot are the average b_2*s* at *0.66, 2* and *4 kA* as derived from the archive data. Since the production measurements in the archive were performed at *~4.6 K* a temperature correction of the data toward a *7%* wider loop width was applied. As explained above this reconstructed hysteretic loop includes an unknown amount of drift and is therefore under-estimating the real case. This feature is indeed clearly visible in Figure 15.

Most of the magnets measured show a standard loop shape, more or less symmetric around the geometric value to which it converges at high current. There are, however, some notable exceptions. In the particular case of TB0269 all magnetic multipoles appear to be distorted at low current. This could be the result of a residual (current independent) magnetization, possibly related to the iron yoke, affecting the multipoles at low current. TC0710 has the particularity that the loop is bent upwards at high current. Most other magnets appear to be bent downwards at high current. This could be the effect of a coil deformation under Lorentz-forces, or the effect of iron saturation.

An important gauge of the quality of the recently acquired data can be obtained from a comparison with the magnetic measurements performed on the same magnets twenty years ago before installation in the tunnel. Therefore a systematic comparison of the 1980 and 2002/2003 data was performed. Any systematic differences potentially indicate issues related to the measurement technique (or changes in the magnet). There are, however, some issues that need to be accounted for in such a comparison: -1- the archive data were not corrected for the drift that occurred between the moment of the current ramp was interrupted and the moment of measurement (these measurements were not done on the fly such as today); -2- the probes used in the 1980 measurements were much longer (*~2.4 m*) than the probes currently used (*~0.83 m*) (the probe length is especially important regarding the effect of longitudinal variations of b_2); –3- the measurement temperature was typically *~4.6 K* in the production measurements and *~4 K* in the recent measurements (as will be shown below this temperature difference is expected to cause *~10%* difference in the loop width). Figure 16 shows a comparison of the body sextupoles measured in the 1980s and recently on three magnets (more magnets would have over-populated the plot). As can be verified in Table 9, the agreement between these measurements is as excellent as in the case of all other candidates.

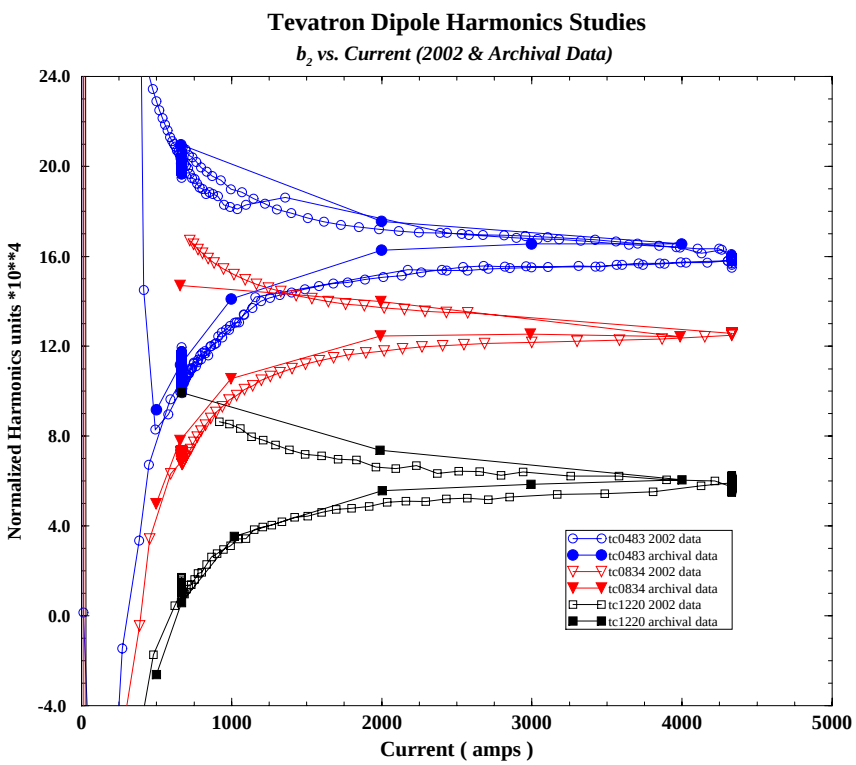

Figure 16: Comparison of body sextupoles measured in TC0483, TB0834 and TC1220 before installation in tunnel and recently. The agreement between these measurements, taken 20 years apart with very different measurement hardware is remarkable.

Table 9: Recent and 20 year old results of measured b_2 loop widths for several Tevatron dipoles recently tested. The b_2 loop width is defined as the difference between the up and down ramp points at 2 kA. Note that the production measurements include an unknown amount of drift (expected to affect the loop width at the level of ~0.5 units). 02/03 measurements were taken continuously on ramp and therefore do no include any drift effects. On the other hand they can include eddy currents effects.

magnet	comment	Hysteretic width at 2 kA (units @ 1")	
		1980s	**02/03**
TC 0483		1.36	2.31
TB 0834		1.53	2.17
TB 0269	"crooked type"	1.07	1.98
TC 1220		1.71	2.74
TC 1052		1.52	2.17
TC 1077		1.60	2.42
TB 1055		1.51	2.31
TC 0525		0.97	2.55
TB 1198		1.87	2.10
TC 0710		1.79	2.32
TC 0504		1.70	2.36
TB 1130	eddy currents ?	0.97	3.72

3.3) End-Body

As discussed in 2) the Tevatron dipole magnets are characterized by a strong, negative sextupole spike in the ends. As shown in Figure 17 for the particular case of Tevatron dipole TC1220, the hysteretic behavior is similar in the ends and in the body. The hysteretic loop measured in the ends can be made to overlap the loop measured in the body, once the difference in geometric b_2 is corrected for. One additional feature of Figure 17 is that it represents the b_2 after normalization on the average dipole field measured in the respective positions. The average dipole field in the ends is lower. Therefore, given the similarity of the hysteretic widths in the body and ends, the absolute sextupole component must also be reduced in the end regions. The fact that the loops overlap, actually indicates that the absolute sextupole component "winds down" in the ends in the same way as the dipole field. Therefore the simplified concept of the magnetic length, which can be used successfully to represent the geometric multipoles, can also be used in the case of the hysteretic multipoles. According to this concept the Tevatron dipole longitudinal b_2 hysteresis profile can be represented with a step-function, where the step occurs at the magnetic length as defined in section 2.3), just in the same way as for the dipole field. Within the magnetic length the hysteretic behavior is that of the body. Beyond the magnetic length there is no hysteretic sextupole. Note, however, that in terms of the geometric sextupole this procedure requires a representation in terms of the end-body average geometric (see column 3 in Table 7). Although not further discussed here, this applies to all Tevatron dipoles.

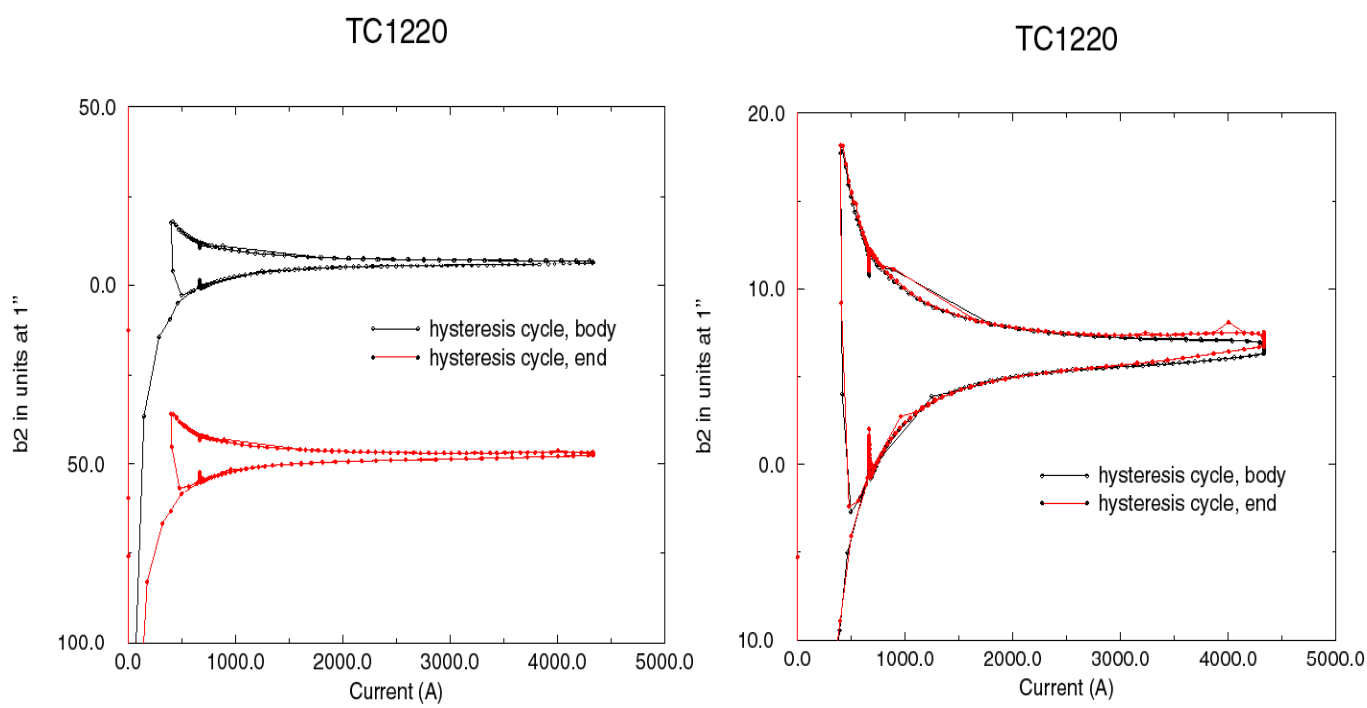

Figure 17: Hysteresis loops in body and end of Tevatron dipole TC1220. Left: as measured, Right: after shifting up the end curve by ~60 units to correct for the difference in geometric b_2. See Figure 5 for definition of body and end position. All measurements were taken at 3.9 K.

3.4) Temperature Effect

It is well known that magnetization effects in superconducting magnets are temperature dependent as a result of the temperature dependence of the critical current density in the superconductor. Apart from the quench performance of the magnets the change of hysteretic b_2 is the major expected effect of magnet temperature variations in the Tevatron. The superconductor magnetization increases with decreasing temperature. Figure 18 shows b_2 hysteresis loops measured in Tevatron dipole TC1052 at two different temperatures, 3.5 and 4.5 K. The two curves can be made to overlap if the larger (3.5 K) is scaled down by 13%. Note that the loops have to be centered on (a geometric of) zero for this procedure to be successful.

Figure 19 shows the result of a calculation of the temperature dependence of the width of the magnetization loop in a Tevatron dipole using ROXIE (more detail on this calculation can be found in [15]). The calculation indicates a linear dependence in the temperature range 2-5 K, with a slope of –16.8% per deg K with respect to the Tevatron operating point of 4 K. The linearity of the temperature dependence of the magnetization in the temperature range of interest (3.5 - 4.5 K) simplifies the predicted effect of temperature variations on the b_2 correction in the Tevatron. The Tevatron currently, however, does not take into account temperature variations in the b_2 correction procedure. It is assumed that the temperature in the Tevatron magnets is the same from shot to shot.

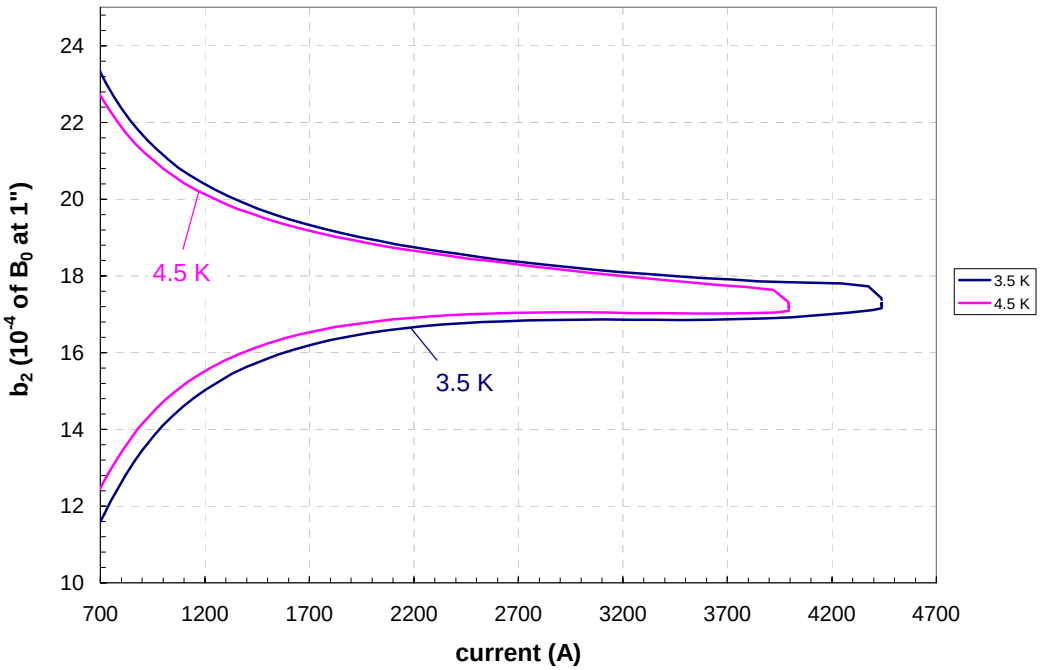

Figure 18: Hysteretic loop measured in the body of TC1052 at 3.5 K and 4.5 K. The measurement was performed during the 1996 dynamic effects measurement campaign [1].

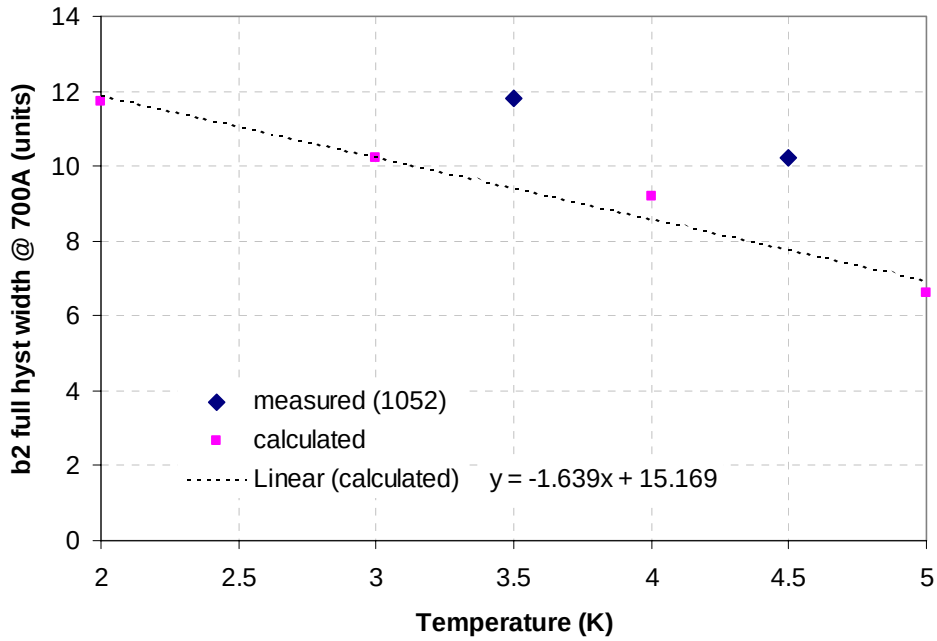

Figure 19: Temperature dependence calculated with ROXIE and compared to the measurement shown in Figure 18.

3.5) Eddy Current Effect

Eddy currents can affect the hysteretic multipoles and in particular b_2 also. One of the standard textbooks on superconducting accelerator magnets[4] states that in the Tevatron dipoles the b_2 hysteresis full width at injection related to a ramp-rate of *10 A/s* (and an average contact resistance in between strands in the cables forming the coils of 10 μΩ) is expected to be 0.61 units. This would be a noticeable effect. Measurements performed on two Tevatron dipole magnets reported below (Figure 20) indicate an effect of ~0.1 units on the full width of the hysteresis loop at injection at the peak ramp rate in the Tevatron (70 A/s). Assuming a linear dependence of the b_2 full hysteretic width on ramp rate and a 1/x dependence on contact resistance this is consistent with the textbook value if the contact resistance in the Tevatron cables is *~200 μΩ*. This is a relatively large contact resistance, but more or less expected because the Tevatron cables use a so-called zebra-design, with every second strand having a Ebonol coating that increases the contact resistance significantly. Also shown in Figure 20 is that the hysteretic width actually decreases with ramp-rate. This is expected for the b_2 in superconducting dipoles with a substantial hysteretic width due to superconductor magnetization because the eddy current b_2 hysteresis is opposite in sign to the superconductor magnetization contribution.

[4] P. Schmueser, K. Mess, S. Wolf, "Superconducting Accelerator Magnets", World Scientific

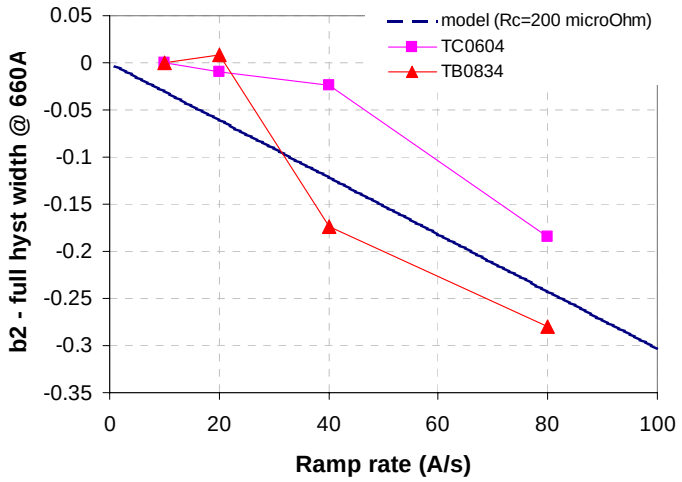

Figure 20: Measurement of eddy current effect on hysteretic loop (full) width at 666 A (injection) in Tevatron dipoles TC0604 and TB0834. Also shown is a model calculation based on Devred[4].

We therefore conclude that eddy-current effects do not affect the magnet sextupole at a level exceeding 0.1 units even at the highest ramp-rates in the Tevatron.

4) Dynamic b2

4.1) Analysis Procedures

The typical sextupole (b_2) hysteresis loop from the nominal measurement is shown in Figure 2. In the Tevatron operational scheme the main magnet hysteretic and dynamic sextupoles are compensated separately. To separate the dynamic from the hysteretic and geometric effects the following data reduction procedure was applied. We find the linear fit of b_2 as a function of the current in the region of *0.7-0.78 kA* and extrapolate its value back to the injection current *0.66 kA* (Figure 21). This defines the so-called baseline that we then subtract from the data. After the baseline subtraction the snapback returns to zero. Another information needed is the exact time of the start of the injection porch. We obtain this information via identification of the start of the ramp from the injection porch and subtraction of the nominal injection porch duration. The time at which the ramp starts is found with a procedure in which the part of the current profile is found into which a parabolic function can be fitted. This procedure takes advantage of the fact that the ramp is purely parabolic only during the first *~6 sec*.

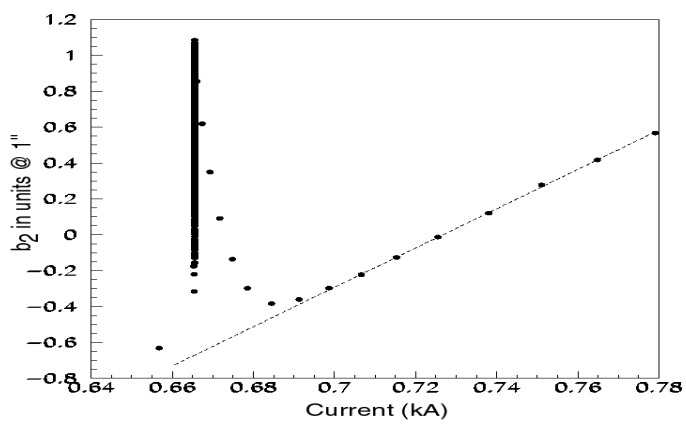

Figure 21: Snapback and the line approximation of the loop in the snap-back region used for the data base-line correction.

As will also be apparent in many of the following drift plots the drift does not necessarily start at zero, but scatters around a certain offset. The offset is possibly the result of very fast drifts in the first few seconds of the injection porch or the effect of current overshoots. This is an issue that is still being investigated at the moment. As explained in the following we believe that the random variations are an artifact of the measurement technique. The length of the tangential coils in the rotating coil probe is *81.7 cm*. The measured period of the periodic pattern in Tevatron dipole presented in 2.5) is *6.2 cm*. Therefore the probe covers *13.2* pattern periods. In the worst case (assuming a pattern amplitude of *10 units* peak to peak) the pattern effect in the rotating coil measurement can be *0.03 units* (in the best case zero). In the case of the Hall-probe measurements the effect is calculated differently but can be ten times larger in the worst case.

$$\left|\Delta b_{2,\,pattern}\right| = \frac{b_2^{peak}}{2\pi}\frac{L_{pattern}}{L_{probe}}\left(1-\cos\left(2\pi\frac{L_{probe}}{Lpattern}\right)\right) \tag{6}$$

As will become very clear in the following the most important aspect of the dynamic effects in superconducting magnets is that they depend on the previous powering history of the magnets. One of the reasons why the Tevatron runs through a beam-less pre-cycle before every physics run is to repeat the same powering history (a ~ 1 hr pre-cycle suffices since the "memory" of the magnets appears to be ~hrs). The pre-cycle parameters become the important history parameters. As shown in Figure 6 the Tevatron accelerator cycle foot-print is characterized by the so-called front-porch (FP), flat-top (FT), back-porch (BP) and injection porch (IP). These abbreviations will also be used extensively in the following.

4.2) Drift

4.2.1 Parametrization of the b2 dependence on time

Two different functional forms have been used in the past to model decay processes in superconducting accelerator magnets. The behavior of Tevatron and HERA magnets could be modeled as a logarithmic decay [17],[18].

$$\Delta b_2 = b_{2,0} + b_{2,1}\cdot\log(t/t_0). \tag{7}$$

The behavior of RHIC magnets was parametrized by two superimposed exponentially decaying terms [19]

$$\Delta b_2 = b_{2,0} + b_{2,1}\cdot e^{-t/t_1} + b_{2,2}\cdot e^{-t/t_2}. \tag{8}$$

In our case we used a logarithmic function to parametrize the b_2 decay. It was found that t_0 is close to *1 s* as in the HERA magnets thus $t_0 = 1\ s$ was fixed in our fits. To describe the interval below *100 s* we slightly modify the logarithmic form (7) adding a time offset parameter t_s

$$\Delta b_2 = b_{2,0} + b_{2,1}\cdot\log(t+t_s). \tag{9}$$

In the parametrizations (7,9) the time variable is set to zero $t=0$ at the beginning of the injection plateau. However, the parameter $b_{2,0}$ has no meaning at $t=0$. This is why we recently modified the form (9) to

$$\Delta b_2 = b'_{2,0} + b_{2,1}\cdot\log\left(\frac{t+t_s}{t_s}\right). \tag{10}$$

In this form after subtraction of the hysteresis loop $b'_{2,0}$ should be close to zero and at $t=0$ $\Delta b_2=0$ consistent with the expectation from the current understanding of the decay process. As will be shown in the following the drift parametrization (10) works very well in Tevatron dipoles in the time frame 1-600 mins. It appears, however, that $b'_{2,0}$ often is not zero in the Tevatron dipoles. This issue is currently under investigation. A fast drift occurring at the second time scale such as due to regular eddy currents or demagnetization effects due to current overshoots are the avenues of explanation being pursued for the moment. Once this effect is better understood, new terms might have to be added to (10).

Another possible source of $b'_{2,0}$ could be the effect of the imperfect integration over the field pattern with the probe length being a non-integer multiple of the pattern period. This effect, however, is estimated (see section 4.1)) to give a negligible contribution (*~0.05 units)*.

The form in (10) will be used to parametrize the decay versus time in the cases of different pre-cycle parameters. Figure 22, for instance, shows the b_2 decay for different durations of *FT*.

The parameters $b_{2,1}$ and t_s were fitted with different functional forms, either polynomial or exponential or a superposition of both, depending on the duration of *IP*, *BP* and *FT*. These one-dimensional functions are the first step towards a possible new multi-parameter correction form for the Tevatron b_2 correction at injection. We also tried to model the b_2 decay with a double exponential form according to (8) on four of the measured magnets. In two of them the fit returned a very large time constant of the order of 10^6 *sec*. In the other two magnets the double exponential form (8) performed slightly better than (9). The attempt to find the best parametrization for the decay part is not conclusive at this point and will be continued in the future experiments and analysis. As mentioned above, one such issue being further investigated is that of very short time constant contributions. In addition we are trying to understand if there is a reason for the different parametrization behavior (for example as a result of different cable characteristics). Our proposal, see the conclusions of this report, is to use the form (10) to correct the sextupole decay during the injection plateau and tune the parameters $b_{2,1}$ and t_s using beam measurements.

4.2.2 Decay amplitude vs duration of flattop

Typical decay curves for different *FT* durations are shown in Figure 22. The measurements include varying *FT* durations from *1 min* up to *12 hrs*. One can conclude that after one hour of *FT* the b_2 decay slope reaches saturation. This result is at the basis of our proposal to remove the short pre-cycles after successful (=intentionally aborted) stores in the Tevatron [9]. Figure 23 summarizes the parametrization of the $b_{2,1}$ and t_s as a function of the *FT* duration. A simple exponential form was used to fit the slope and time offset defined in the logarithmic form (10). The dotted magenta curve represents the simultaneous fit of all magnet data. The conclusion is that slope parameter $b_{2,1}$ (left)

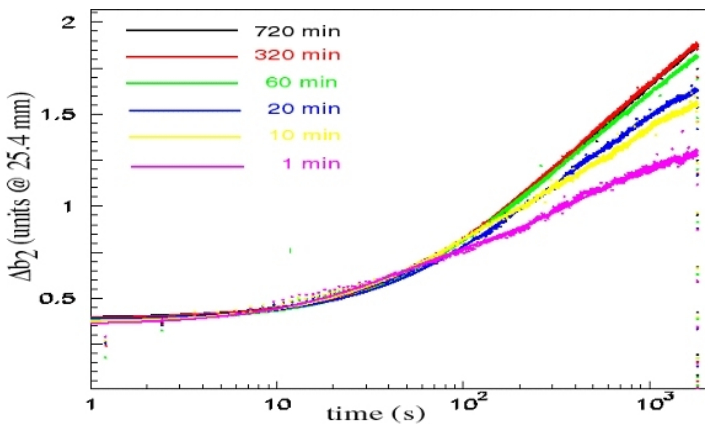

Figure 22: Decay of the sextupole component for a plateau at injection of 30 min. and different duration of FT in TC1220. After a one-hour duration of FT, the b_2 decay shows similar (green, red and black) behavior.

increases up to *60 min FT* duration and after this it shows a flat tendency. On the other hand the time offset t_s shows little or no dependence with *FT* duration, except for the earliest measurements of TB0834, which were of lesser quality than the subsequent measurements.

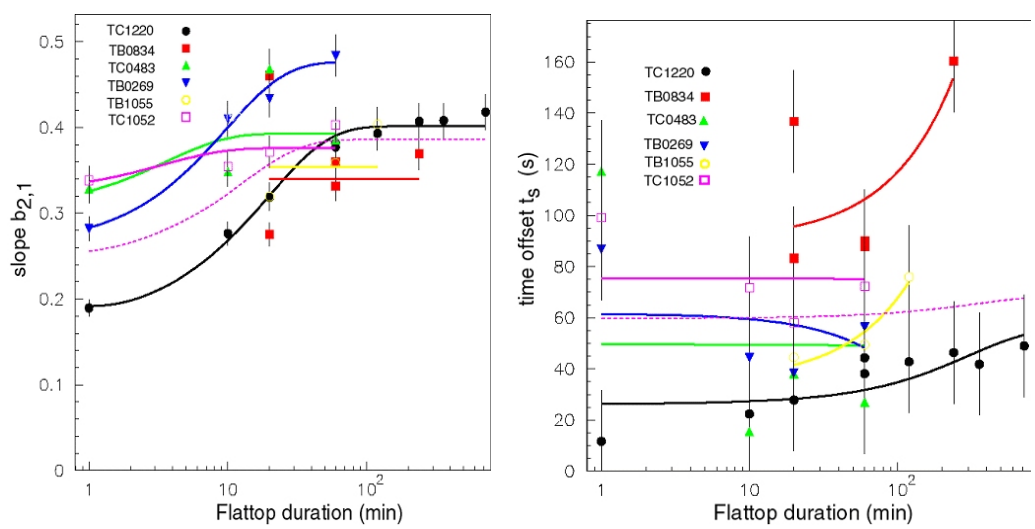

Figure 23: Slope $b_{2,1}$ (left) and time offset t_s (right) for different FT durations. The dotted magenta line represents the simultaneous fit of all data.

4.2.3 Decay amplitude vs duration of backporch

The backporch duration has a strong influence on the decay amplitude. A similar result was obtained from the 1996-1997 measurements performed on two Tevatron dipoles [1]. In detail, the change of decay/snapback amplitude will be discussed in another section below together with the corresponding snapback time. The decay curves for different durations of the *BP* are shown in Figure 24. One could observe that changing the *BP*

from *1* to *5 min* decreases the decay amplitude by ~45 %. Our parametrization form (10) does not describe the decay curves in the first *10 sec*. In some cases better parametrization in the beginning of the decay is achieved with two exponential fits performed with functional form (2). Figure 46 shows the slope parameter and the time offset vs the *BP* duration.

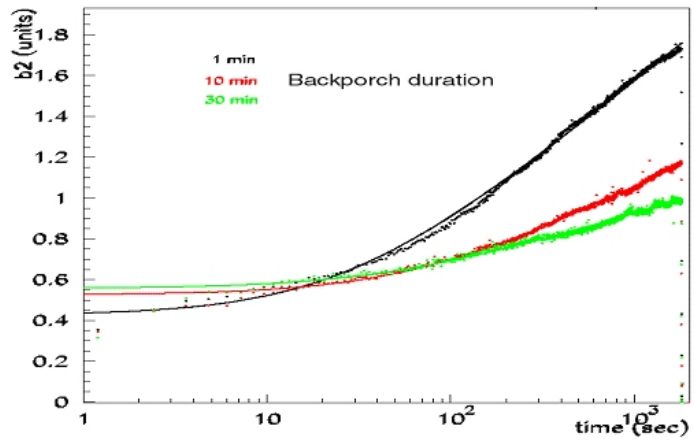

Figure 24: An example of decay vs BP duration plot for the magnet TC1220.

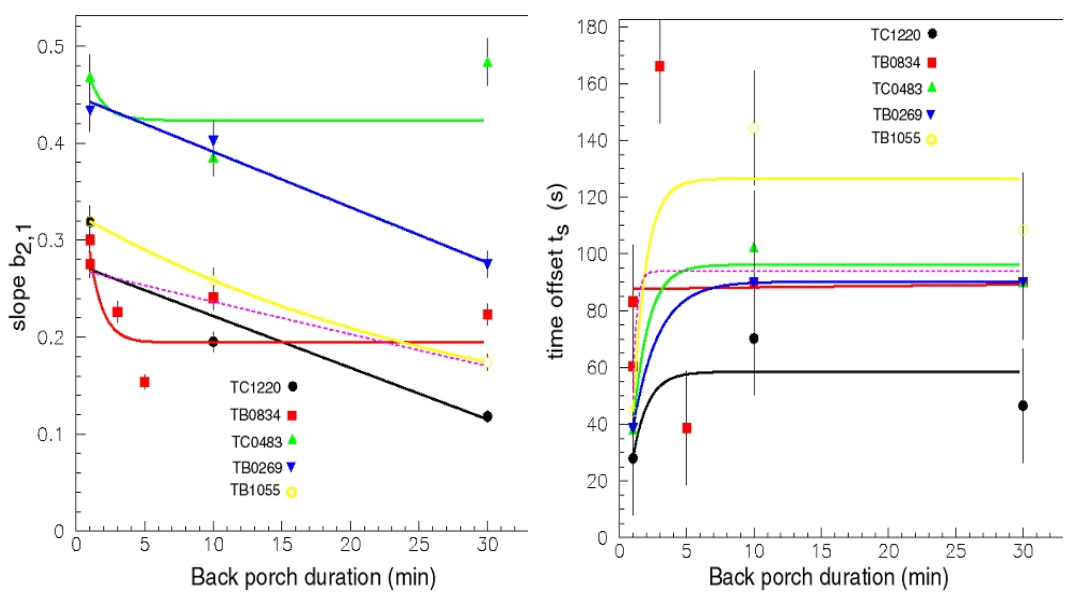

Figure 25: Slope $b_{2,1}$ (left) and time offset t_s (right) for different BP durations. The dotted magenta represents the simultaneous fit of all data.

4.2.4 Decay amplitude vs number of flattops

A detailed measurement of the decay amplitude vs *NFTs* (pre-cycles) was performed on four Tevatron dipoles. The executed current cycle corresponded to our standard one (*FP=1, FT=20, BP=1, IP=30 min*) where we repeated the first part of the cycle (*FP, FT, BP*) up to six times.

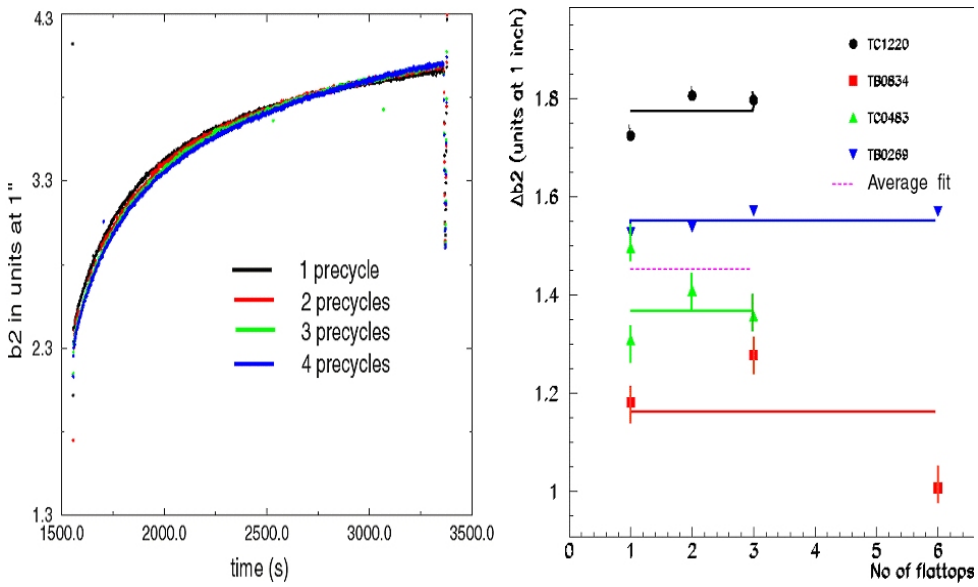

Figure 26: Left: the sextupole decay for different NFT for TB0269. Right: the decay amplitudes for the four measured Tevatron dipoles as a function of NF are shown. The dotted magenta line represents the average fit.

The result for the magnet TB0269 is shown in Figure 26 (left). Small shifts of the order of *0.08-0.12 units* were applied to the decay curves in the cases of *2,3* and *6* flattops to remove differences in offset. These shifts were calculated from the corresponding hysteresis loops normalizing them to the values in the region *I=0.70-0.78 kA*. They might be explained as possible field fluctuation due to superconducting cable twist pitch (a.k.a. pattern effect). Figure 26 (right) summarizes the decay amplitudes vs number of pre-cycles for the four measured magnets. The data show a relatively flat distribution and a constant describes our measurements with a good probability (~16%).

4.2.5 Decay amplitude vs the maximum flattop current

In Run II Tevatron operation the maximum current is held constant at *4333 A*. This corresponds to a beam-energy of *980 GeV*. For a more complete decay characterization we performed several measurement with different flattop currents of *3552, 4000* and *4333A*, which correspond to *800, 900* and *980 GeV* beam energy in the machine. The result confirmed the previous observation, based on the 1996-1997 measurement of one dipole (TC1052) [1], that there is a relatively strong dependence of the decay amplitude on the maximal flattop current. Figure 27 shows the decay in cases of the above mentioned currents and otherwise standard durations of the ramp porches (*1,20,1,30*).

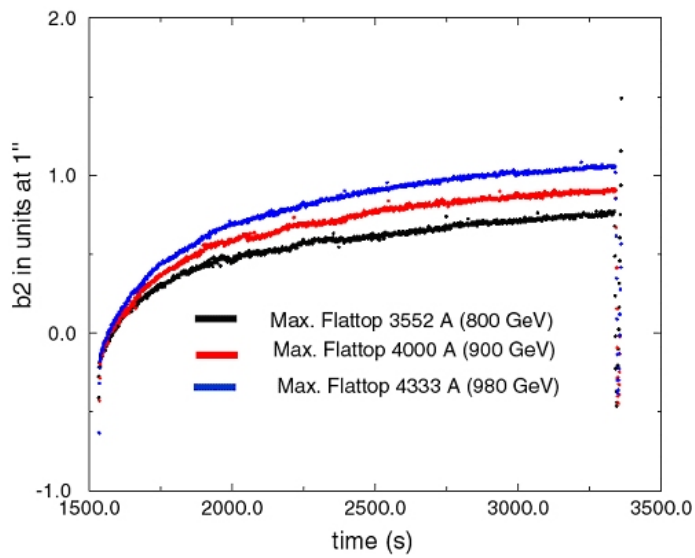

Figure 27: Sextupole decay and snapback as a function of the maximum flattop current in TC1220. The variation in the maximum current gives the third largest effect to the decay amplitude after the BP and FT durations.

4.2.6 Decay amplitude vs duration of frontporch

We measured the decay behavior versus the duration of the front porch in one dipole (TB1055). The overlaid hysteresis loops in cases of the *1 min* and *60 min* front porches are shown in Figure 28. No change in the decay behavior is apparent.

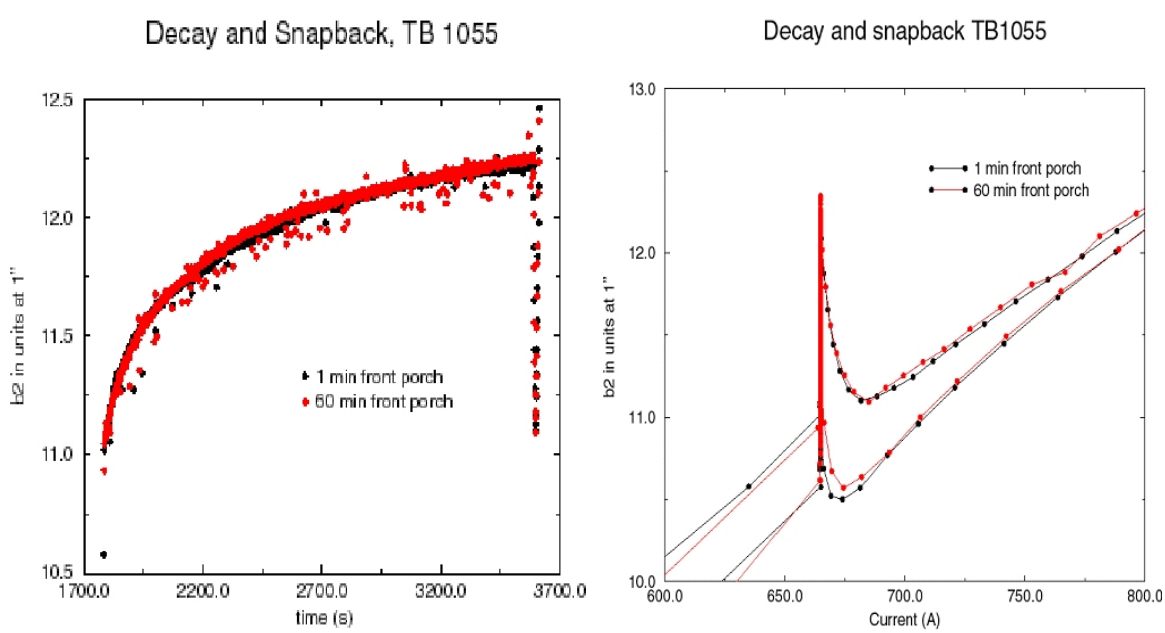

Figure 28: Sextupole decay and snapback with a part of the hysteresis loop in case of 1min and 60 min front porch durations. Left: The decay vs time for the same measurement.

4.2.7 Comparison of the decay in body vs end and body vs body

Measurements comparing the decay amplitudes between different positions in the body and between the body and the end of the magnets were performed in several Tevatron dipoles. Apart from the expected differences in geometric b_2 (see discussion in 2.4) the curves match after the geometrical shift is removed. Figure 29 shows the sextupole drift in the body and end of TC1220 and in different body positions of TC0525.

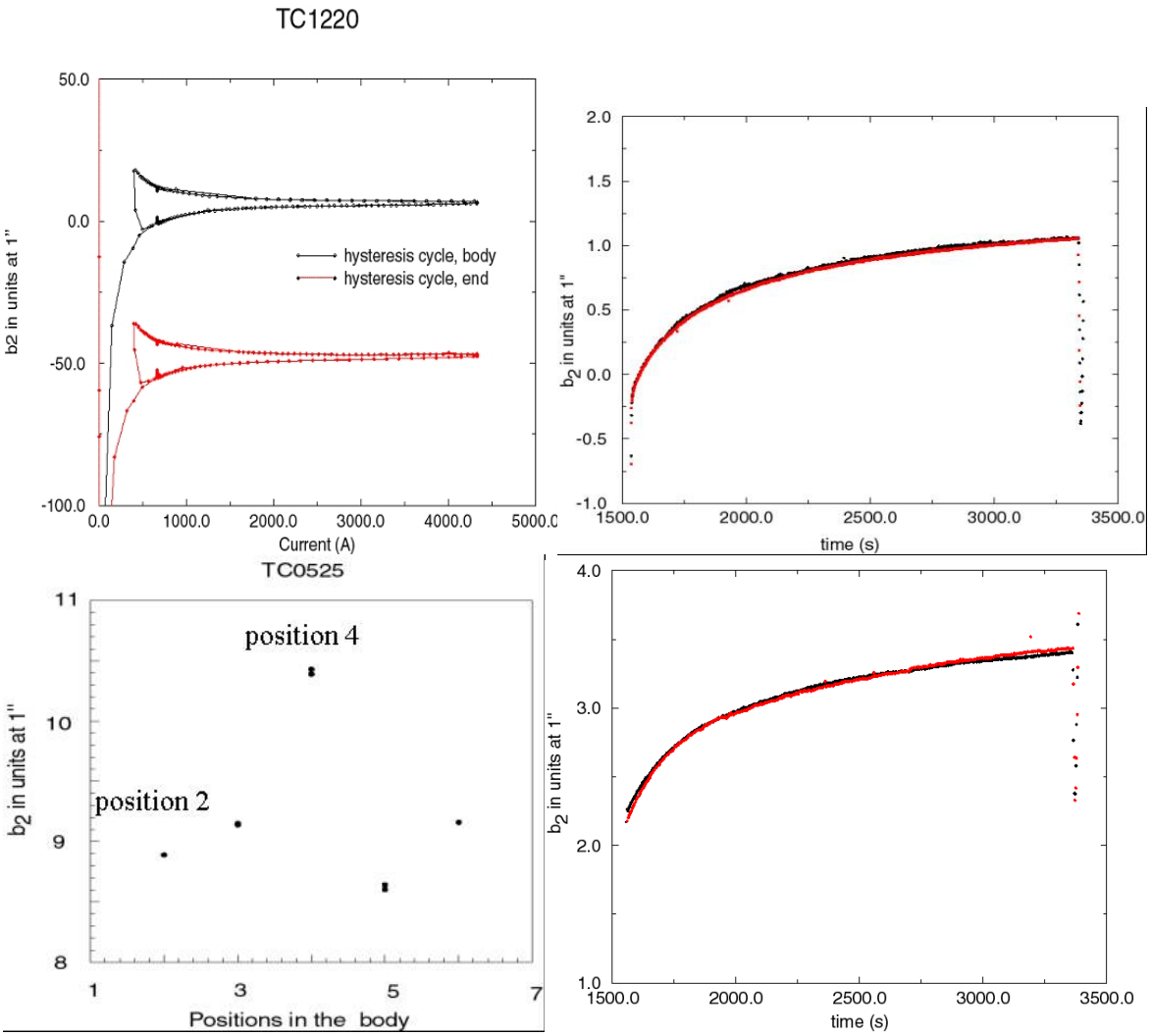

Figure 29: Left top: Sextupole hysteresis for the body and the end. The large difference between the ends and the body of Tevatron magnets is imposed in the design. Right top: The same plot when the decay curves are overlaid. Left bottom: the variation of the sextupole at 4.3 kA in the TC0525 body. The maximal observed b_2 variation is ~2.0 units. Right bottom: the decay curves for the longitudinal positions 2 and 4 in the TC0525 body after overlaying.

4.2.8 Temperature dependence of the decay

As discussed in detail in 3.4) the width of the b_2-hysteresis loop in the superconducting magnets depends on the temperature. Dedicated measurements in the Tevatron dipoles TB0834 and TC1052 showed a temperature dependence of approximately *16%* and *13%* per *1 K*. A typical example of b_2 hysteresis loops at different temperatures is shown in Figure 18.

The question was posed if the decay and snapback, which are de- and re-magnetization effects, are also scaling with the magnet temperature. Figure 30 shows the b_2 drift in TB0834 following a *1-20-1* pre-cycle at *4.1 K, 4.4 K* and *3.8 K*. If one takes into account the change of the hysteretic baseline for these three cases (*0.3* and *0.73* units respectively to "normalize" the *4.1 K* and *4.4 K* baseline to the *3.8 K* case), they agree very well (right plot in Figure 30). We therefore conclude that there is no significant change in the decay profile with temperature.

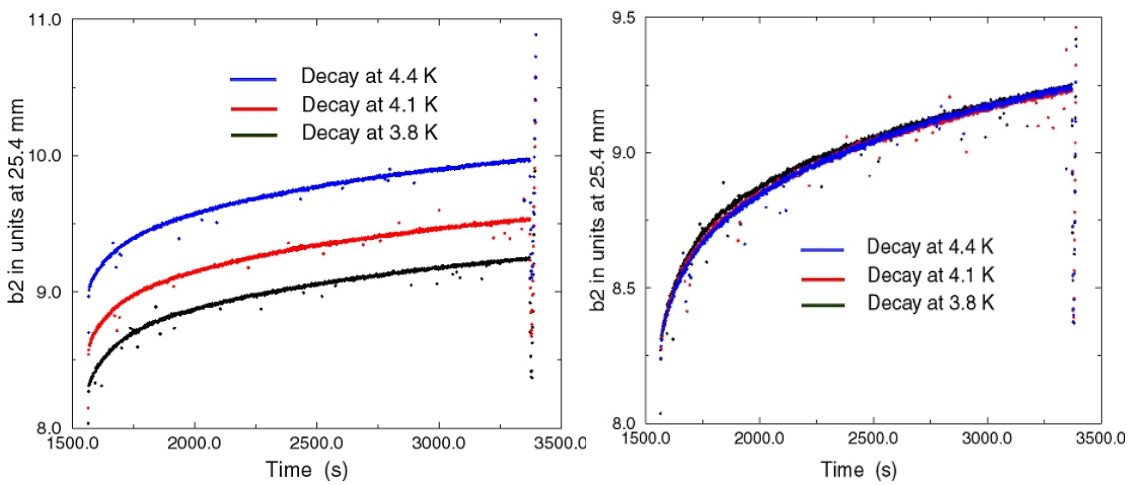

Figure 30: Decay and snapback of the sextupole component for a plateau at injection of 30 min, the flat-top duration of 20 min, and back-porch duration of 1 min in TB0834. Left: before shift; Right: after shift to account for difference in hysteretic b_2 baseline. The different colors represent the decay at different magnet temperatures.

4.2.9 Special case: FT 60 min, BP 5 min and variable IP

For one magnet, TB0834, we performed special measurements with fixed duration of *FT =60 min* and *BP=5 min* (*FP=1/FT=60/BP=5 min*), and a variable injection time of *30,60,120,180,240 min*. These *FT* and *BP* durations are the new standard pre-cycle parameters for the Tevatron operation (one of the results of this work, more details in [9]). Performing these measurements we checked how accurate the functional form (10) describes the decay amplitude vs time. Typical examples of the decay parametrization in the cases of a *60* and *240 min* injection plateau are shown in Figure 31. Figure 32 summarizes all the fits performed for different durations of the injection plateau. The fit parameters are listed in Table 10. The average values obtained from these fits are $b_{2,1}$ = *0.3837+/-0.030 units* and t_s = *328.3+/- 89.2 s* respectively.

Table 10: Fit parameters in case of different duration of the injection plateau.

Injection time (min)	$b_{2,1}$ (units)	t_s (s)
30	0.370589	310.26
60	0.409611	397.22
120	0.4259	437.22
180	0.3721	281.37
240	0.3402	215.8

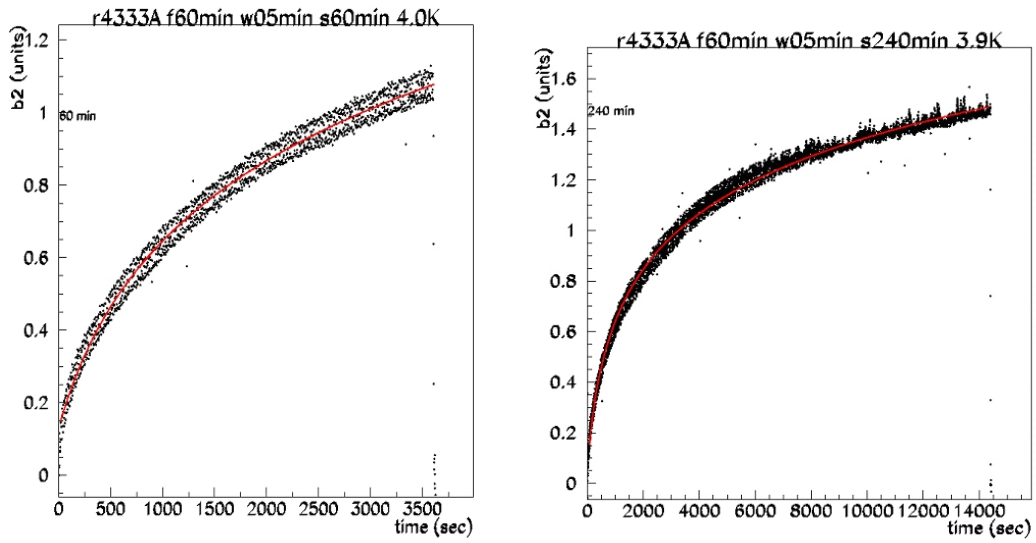

Figure 31: Decay of the sextupole component in TB0834 for a FT duration of 60 min, BP of 5 min and different durations of the injection plateau: left plot 60 min, right plot 240 min. The red line represents the fit with (4).

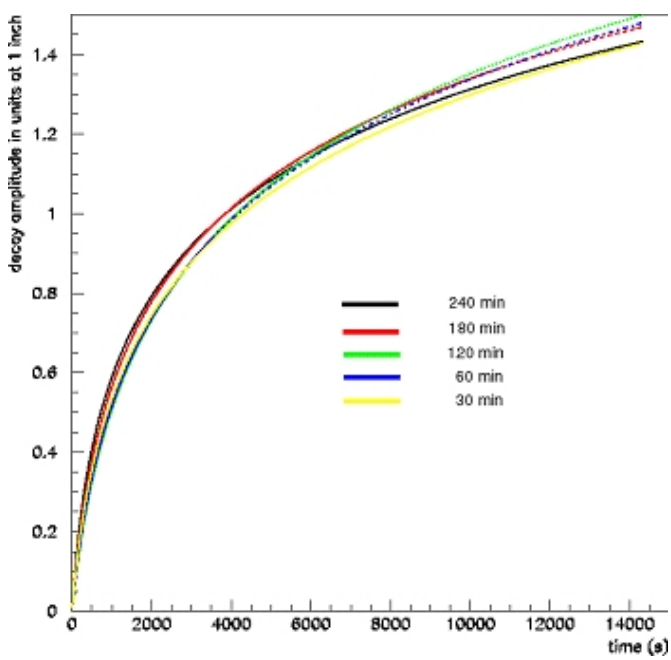

Figure 32: Parametrization of the sextupole component decay for a FT duration of 60 min, BP of 5 min and different durations of the injection plateau.

4.3) Snap-back

4.3.1 Parametrization of the snapback amplitude

At the Tevatron the snapback compensation is done according to

$$\Delta b_2 = b^s_{2,0} \cdot (1 - t^2 / t_0^2)^2, \tag{11}$$

where $b_{2,0}$ is the initial amplitude and t_0 is the snapback time [1]. Although the polynomial form (11) was found to work for the snapback compensation, we determined that a Gaussian form

$$\Delta b_2 = b^s_{2,0} \cdot \exp(-t^2 / t_0^2), \tag{12}$$

describes our measurements with better accuracy. The time scale is set to zero when the acceleration ramp is started and the snapback is initiated. Note that t_0 has a different meaning in formulae (11) and (12): in the first case it is the value where the functional form is zero-ed, in the second case, it is the standard width of the Gaussian distribution. Why a Gaussian form? A common parametrization for the snapback curves is considered to be exponential function of the increase of the dipole field ΔB_0 during snapback (see ref. [10] for more details).

$$\Delta b_2 = b^s_{2,0} \cdot \exp(-\Delta B_0 / \Delta B_{snbck}), \tag{13}$$

However, at low currents, including at injection, ΔB_0 is proportional to the excitation current. In the case of the Tevatron, the first ~*15 s* of the current ramp are parabolic ($I = I_{snbck} + \alpha t^2$), and $\Delta B_0 \propto \alpha t^2$. Substituting the time dependence of ΔB_0 in (13) we obtain the Gaussian form (12).

Unlike the drift, the snapback happens fast and is therefore unaffected by a change of the periodic pattern. It is therefore more reliable to derive the drift amplitude from the baseline corrected snapback than from the drift itself. We could have chosen to parameterize the drift amplitude with equation (10), but chose to use an exponential form as in (14). We parametrized the snapback amplitude $b_{2,0}$ and time t_0 as a function of the duration of the current cycle intervals (*IP, BP, FT*).

$$b_{2,0}, t_0 = p_1 \cdot \exp(-t / p_2) + p_3 \tag{14}$$

where t is the duration in minutes of the specific porch is proposed.

4.3.2 Snapback amplitude and time vs duration of flattop

Typical snapback fits measured on TC1220 are shown in Figure 33. One can observe that after *40-60 min* of *FT* the snapback amplitude and duration after 30 min at the injection porch become practically independent of *FT* duration. Figure 34 shows fits of $b_{S2,0}$ and t_0 with the exponential form (14) for different durations of the *FT*. The dashed line represents the average fit of the data measured in five magnets. This result is important for the optimization of the Tevatron operation. In fact one can propose to remove the existing pre-cycle(s) after the

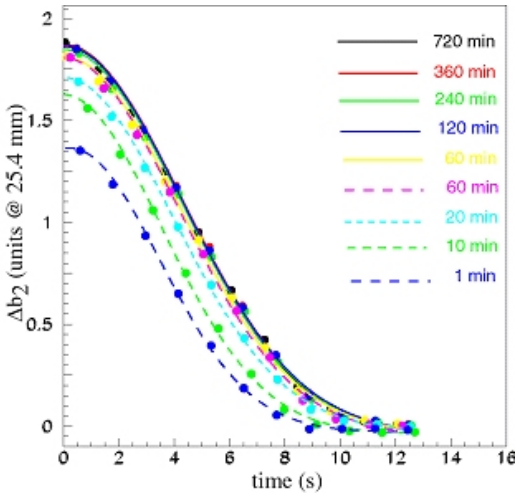

Figure 33: Snapback of the sextupole component for a plateau at injection of 30 min and different durations of the flat-top in TC1220. The dashed lines represent the snapback for short flat-top durations.

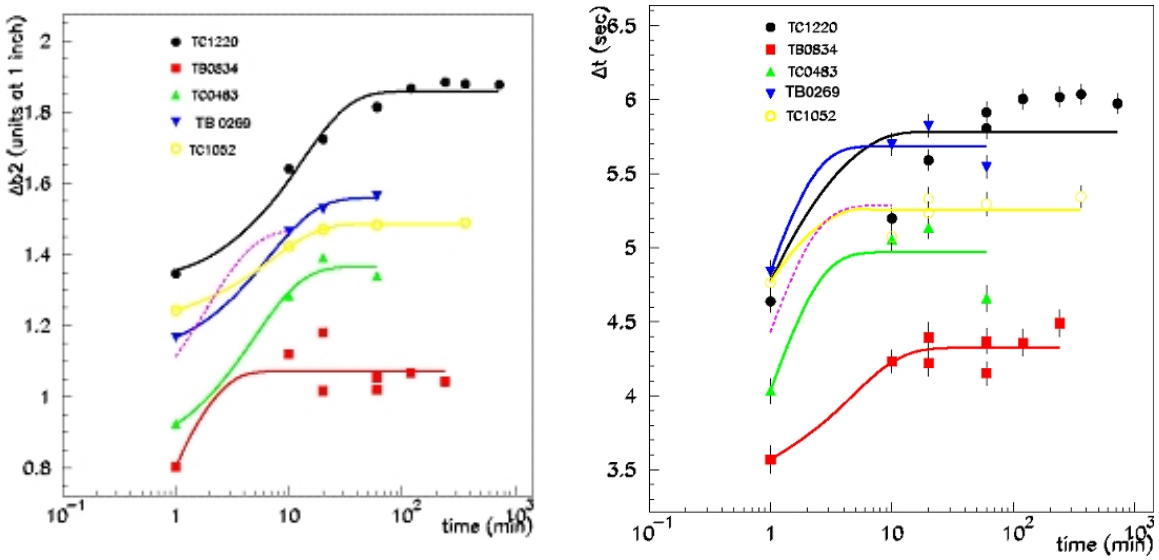

Figure 34: The snapback amplitude and time (after 30 min at IP) parametrized with (14) as a function of the FT duration. The dashed line represents the average fit for the sample of five magnets.

end of a successful store and to start the injection directly after ending a collision. In this case the previous store in effect becomes the pre-cycle for the next stores, implying long *FT* conditions.

4.3.3 Snapback amplitude and time vs duration of backporch

The effect of the *BP* duration on the dynamic b_2 is contrary to that of the *FT* duration. The snapback amplitude and time decrease exponentially with the *BP* duration. This tendency is shown in Figure 35, where the snapback curves after a 30 min IP in the cases of a *20 min FT* (left) and a *60 min FT* (right) for different *BP* durations (*1,10* and *30 min*) are shown.

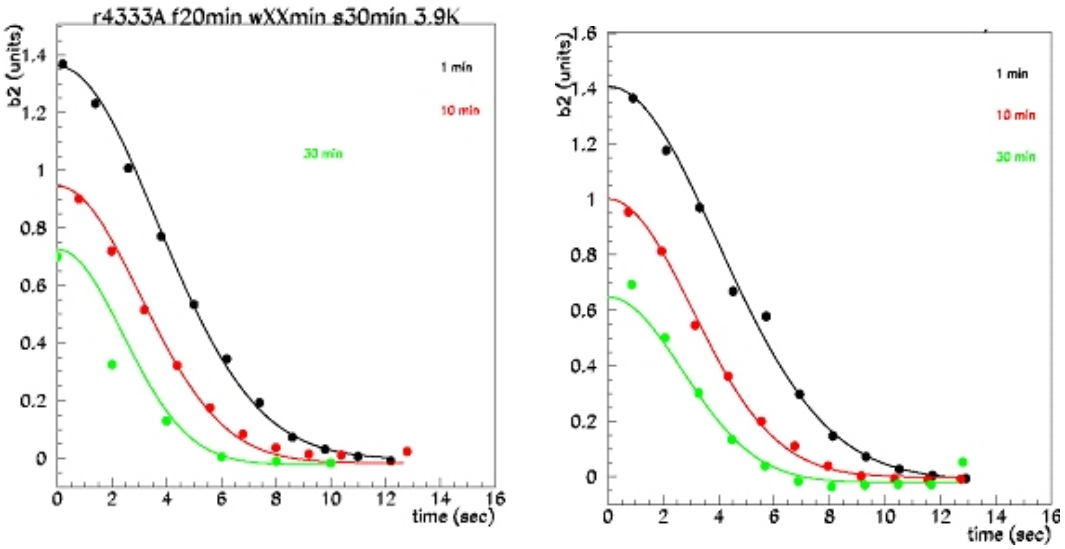

Figure 35: Snapbacks after 30 min at IP measured in magnet TB1055 after a 20 min FT (left) and 60 min FT (right) and BP durations of 1,10 and 30 min.

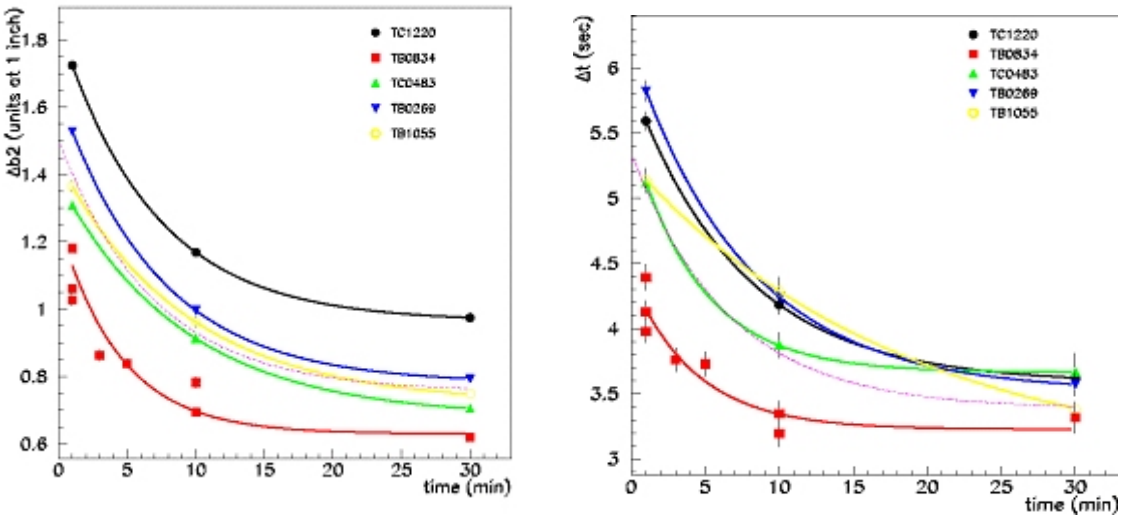

Figure 36: The snapback amplitude and time after 30 min at IP, parametrized with (14) as a function of the BP duration. The dashed line represents the average fit for the five magnets.

Figure 36 shows the $\Delta b_{S2,0}$ and t_0 parametrizations with the exponential form (14) for different duration of *BP*. The dashed line represents the average fit to the five measured magnets. One can see that the average values of Δb_2 and t_0 strongly depend on the *BP* duration in the first *1* to *10 min*. However, Δb_2 and t_0 converge to *0.8 units* and *3.5 s* respectively at large values of the *BP* duration. A possible conclusion for an optimization of the Tevatron operation, which prefers short (*3-10 min*) *BP* durations, is to fix the length of the *BP* plateau. This will decrease the number of variable parameters for the sextupole component decay and snapback compensation during the injection time.

4.3.4 Snapback amplitude and time vs number of flattops

In Subsection 4.2.4 we discussed the effect of multiple flattops on the decay characteristics. As was mentioned before the executed current profile corresponded to the standard one (*1,20,1,30*) except that we repeated the first part of the cycle (*FP, FT, BP*) up to six times. Typical snapback curves after 30 min at the IP as a result of these measurements for magnet TC1220 are plotted in Figure 37 (left). It obviously shows no dependence of the drift amplitude and snapback on *NFT*. The above conclusion is confirmed with the measurements on three more dipoles. They are summarized in Figure 38. The *NFT* effect is best fitted with a constant. An attempt was made to use a linear approximation in the minimization procedure and it returned negligible slope.

The current procedure in Tevatron operation is to execute up to 6 fast pre-cycles when the store is ended abnormally, mostly due to the magnet quench. A special experiment was performed on magnet TB1055 to confirm or reject the necessity of this procedure. Six one-minute pre-cycles were executed after the magnet was quenched. Figure 37 (right) shows the snapback after 30 min at the IP in this experiment (magenta), compared to those when only one pre-cycle (with varying flat-top duration) was executed. The main conclusion is that after the 6 short pre-cycles the magnet history, which determinates the decay and snapback effects, differs from the history when only one long pre-cycle is executed (which is the case when the store ends normally).

The result could be translated in the following way into an optimization of the Tevatron operation. In case that the store is ended abnormally, for example by a magnet quench, the number of pre-cycles may be reduced from six (as executed now in the Tevatron operation) to one, with a *FT* duration of *40-45 min*. From the point of view of the superconducting magnet history the machine should then be in the same operational state as after a successful store.

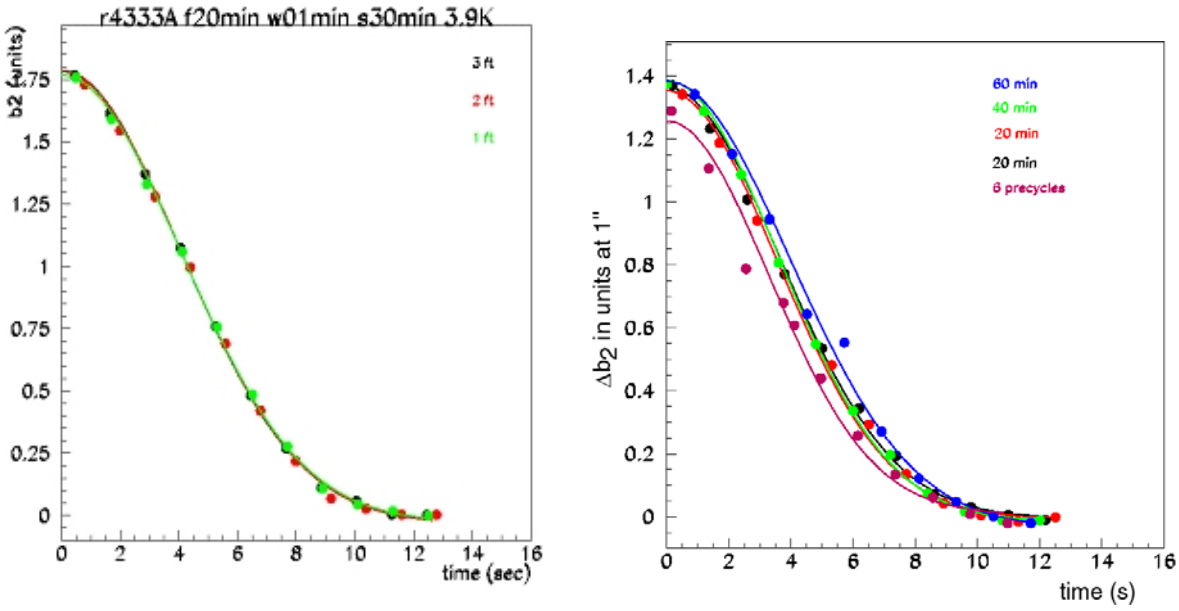

Figure 37: Left: snapback curves after 30 min at IP in case of 1,2 and 3 number of flattops for TC1220. No snapback dependence on NFT is observed. Right: the snapbacks after 30 min at the IP following pre-cycles with 20,40 and 60 min flat-top durations are compared with a special experiment (magenta) in which 1 min pre-cycles were executed 6 times.

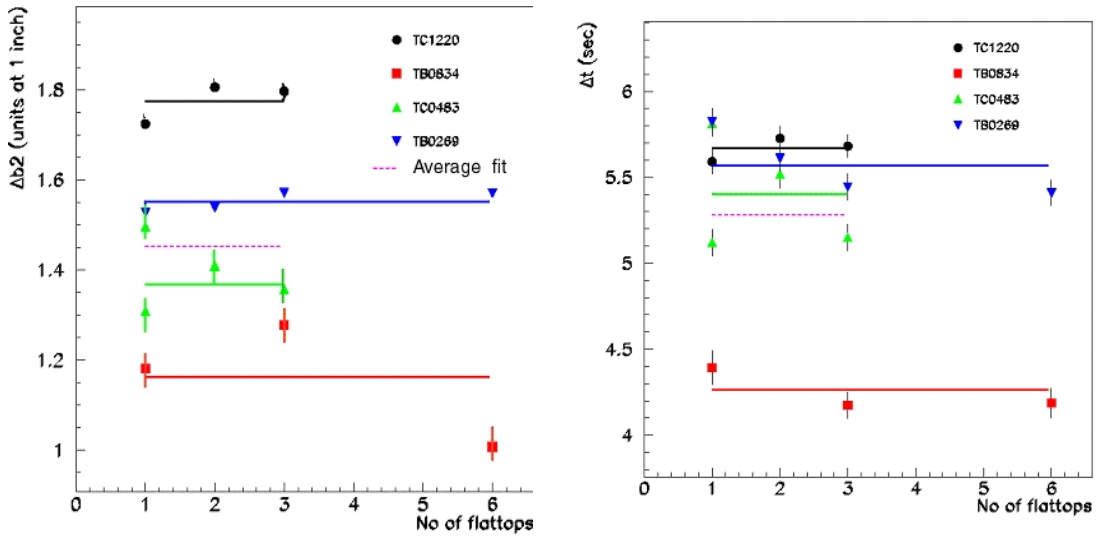

Figure 38: The snapback amplitude after 30 min at the IP (left) and time (right) as a function of NFT. The dashed line represents the average one parameter fit for the sample of four magnets.

4.3.5 Snapback amplitude and time vs maximum flattop current

As was discussed in the Section 4.2.5 the goal of the measurements in which the pre-cycle flattop energy (*FTE*) was varied, was to complete the decay and snapback characterization. The snapback curves for different maximal flattop currents of *3552 A*, *4000 A* and *4333 A*, corresponding to the beam energy of *800, 900* and *980 GeV*, are shown in Figure 39. A strong dependence of the decay/snapback amplitude and time on the maximal flattop current was observed, confirming the result from earlier measurements [2].

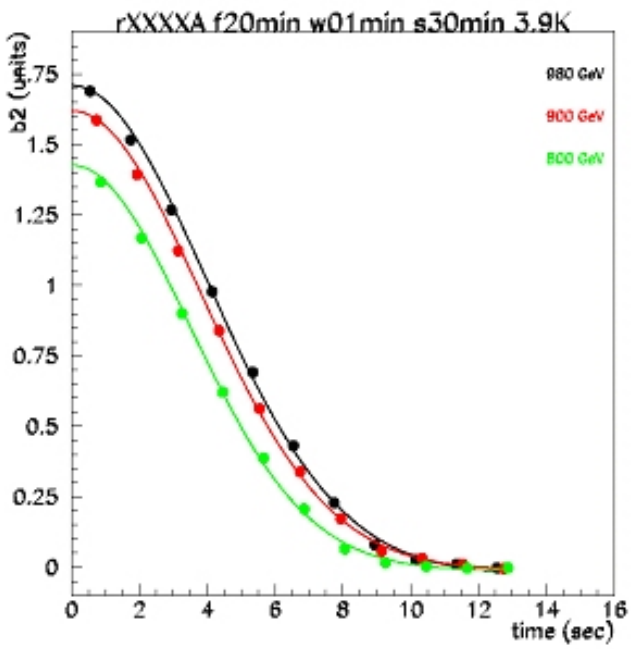

Figure 39: The snapback amplitude and time after 30 min at the IP as a function of the maximum flattop current in the pre-cycle in TC1220. As it was pointed out before, the variation of the maximum current gives the second largest effect on the snapback/decay amplitude following the backporch duration effect.

4.3.6 Snapback amplitude and time vs duration of frontporch

Measurements in Tevatron dipole (TB1055) did not show any significant dependence on the *FP* duration. The overlaid snapback curves after a 30 min IP as a function of time for the *1 min* vs. *30 min* and *1 min* vs *60 min FPs* are shown in Figure 40.

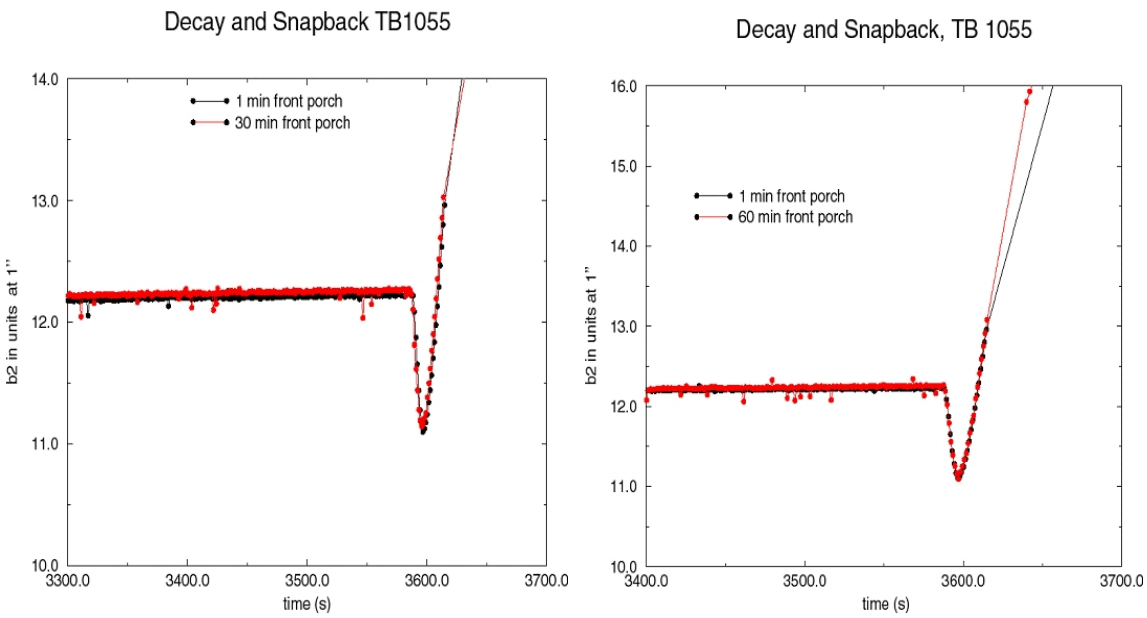

Figure 40: The overlaid snapback curves after 30 min at the IP as a function of time in cases of the 1 min and 30 min (left) and 1 min and 60 min (right) FP. The sextupole amplitudes are not corrected for the hysteresis loop.

4.3.7 Comparison of the snapback for different longitudinal positions

Detailed measurements were executed on several of the Tevatron dipoles in which the snapback amplitude and the snapback time (after 30 min at the IP) between different sections in the body and between the body and the end of the magnets were compared.

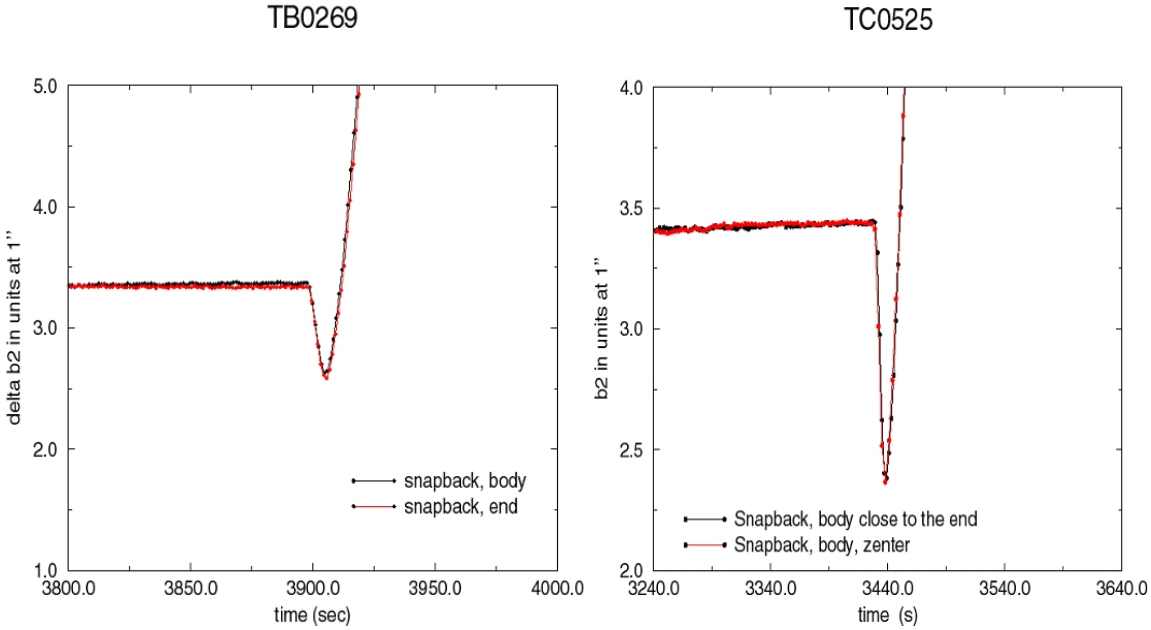

Figure 41: The overlaid snapback curves as a function of time for body and end of TB0269 (left) and TC0525. Note: the sextupole amplitudes are not corrected for the hysteresis loops and the red curves are shifted by ~41 units and ~-0.8 units respectively to overlay with the black ones.

As mentioned before in 2.4) the geometric part of the normal sextupole varies by ~50 units between the body and the end. After shifting the measured end and body data to equalize the geometric component, the snapback curves are in good agreement (Figure 41). We conclude that we do not observe a dependence of the dynamic effects on the longitudinal position in the Tevatron dipoles.

4.3.8 Special case: snapback at FT = 60 min and variable BP duration

The standard measurement program is executed only for three different values of *BP* duration: *1,10,30 min*. Fitting the snapback amplitudes and times with the form (14) one might observe that three measured points are not enough to determine if the exponent (14) describes the data correctly. This is the reason why for TB0834 we performed special measurements with fixed durations of *FP=1 min*, *FT =60 min*, variable *BP* of *1,3,5,10,15* and *30 min* and standard *IP* duration of *30 min*. The result of the parametrization is shown in Figure 42, where in the left plot, the snapback amplitude after 30 min at the IP vs the *BP* duration is presented. The dependence of the snapback time vs the *BP* duration is shown in the right plot. The $\chi^2/ndf(\sigma)$, listed in the upper right corners of the plots, are consistent with high probability (*26%* for the left plot and *21%* for the right distribution) that data and exponential form (14) have the same origin.

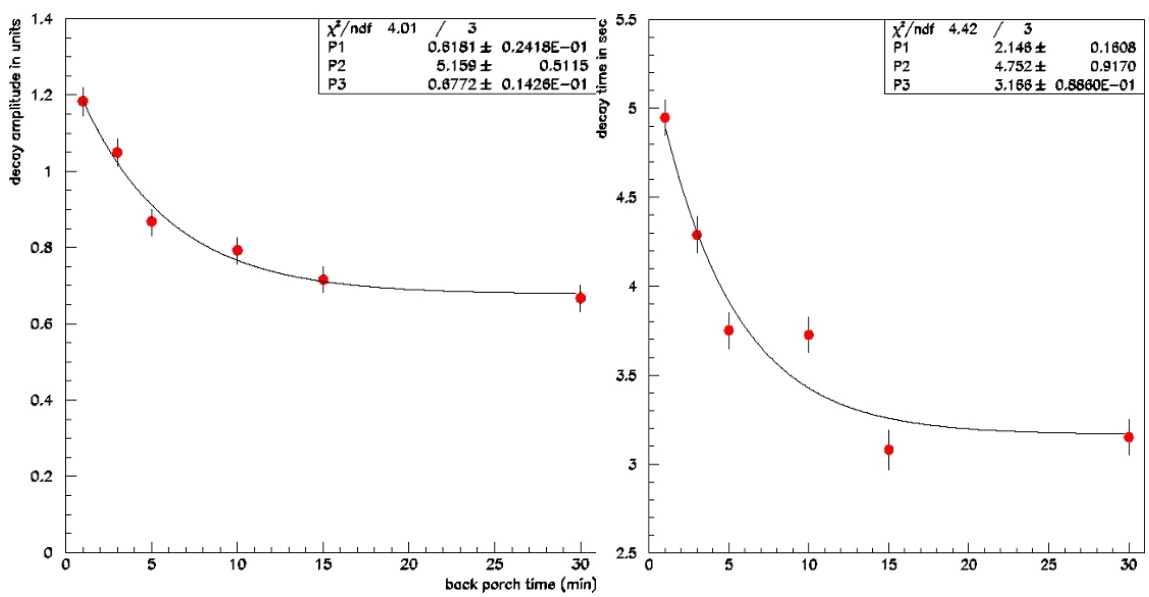

Figure 42: The snapback amplitude (left) and time (right) after 30 min at injection in TB0834 after a 1-20-X pre-cycle and 1,3,5,10,15 and 30 min of BP fitted with (8).

4.3.9 Comparison of Hall-probe and Rotating Coil Measurements

The Hall-probe array with its larger bandwidth was used as an alternate technique for the measurement of the fast snapback. Figure 43 shows a comparison of snapbacks measured with both techniques, showing that the agreement is excellent. Note that the Hall-probe measurements are calibrated on the rotating coil measurements. The calibration, however, is performed with the hysteretic b_2 over the current range of *~0.7-1 kA*, on the hysteretic loop (beyond the snapback). The Hall-probes were most useful for measuring the periodic pattern, in understanding the eddy current effect at the beginning of the injection porch, in measuring the decay and snapback after very short duration of the injection and will be exploited for future measurements where large amount of data are needed for short periods of time.

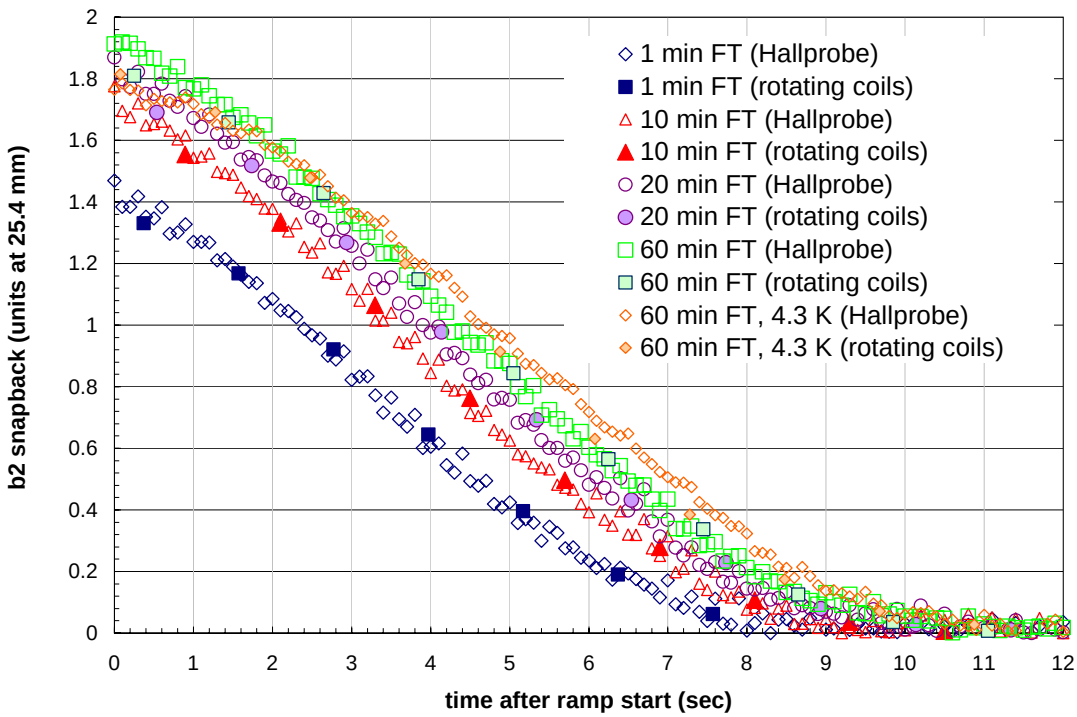

Figure 43: b_2 snapback in TC1220 after 30 min at injection for different pre-cycle flattop durations measured with Hall-probe array and rotating coils. All measurements were performed at 3.9 K except for the 60 min case, which was performed at 3.9 K and 4.3 K.

4.4) Summary of the Effect of Powering History on Drift and Snapback

Table 11 summarizes the fit output for the p_1-p_3 parameters, defined in (14), in cases of different durations of *FT, BP* and different *NFT*. When we vary *NFT* the data are fit to a constant. The errors presented in the table are from the fits and they correspond only to

Table 11: Results from the fits describing $b_{S2,0}$ and t_0 with the exponential form (8). The parameters represent the average fit from a sample of at least four measured magnets.

Par	FT	BP	NF
Snap-back amplitude			
P_1	-0.52±0.11	0.75±0.09	0
P_2	6.40±0.52	6.90±0.23	0
P_3	1.46±0.18	0.75±0.10	1.5±0.2
Snap-back time			
P_1	-2.52±0.16	1.97±0.13	0
P_2	0.81±0.09	6.56±0.22	0
P_3	5.12±0.14	3.38±0.19	5.3±0.2

the statistical fluctuation of the parameters. The expected systematic uncertainties are estimated to be in order of *11%*. This estimation comes from the point-to-point variation of the repeated measurements with the same current cycles and magnet temperatures.

4.5) Correlation between the Snapback Amplitude and Time

To propose a complete scheme of the new Tevatron corrections one should consider investigating the correlation between the snapback amplitude and the time. Obviously this correlation exists: a large amplitude needs a long duration to snapback to the hysteresis loop. A first proposal to establish a functional relation between the snapback amplitude and time was done in [10]. The idea of a linear correlation between the initial snapback amplitude and ΔB_{snbck} was proposed (ΔB_{snbck} is a snapback penetration field, see [10] for more details): $\Delta B_{snbck} = \alpha\, b_{S2,0}$. This linear correlation is also supported by measurements performed at CERN on LHC dipoles. Although ΔB_{snbck} should be equal to zero when $b_{S2,0}$ is *0*, there is no strong evidence that the linearity is conserved for the small values of $b_{S2,0}$ and ΔB_{snbck}. On the contrary, the measurements on the Tevatron dipoles point to a parametrization of the form:

$$b^{S}_{2,0} \cdot = a\Delta B_{snbck} + b. \tag{15}$$

Taking into account the proportionality between $\Delta B_{snbck} \sim \Delta I_{snbck} \sim t_0^2$ (as discussed in 4.3.1) one can establish the desired relation between $b_{S2,0}$ and t_0^2. Figure 44 shows the linear fit with (15) for the full set of measurements performed on TB0834. The origin of the constant *b* in (15) is not well understood.

Figure 45 summarizes a full set of fits with (15) performed on five Tevatron dipoles. An average values of *a=0.149+/-0.01* and *b = 0.391+/-0.03* are shown in the right boxes of the plots. The quoted errors are only statistical ones.

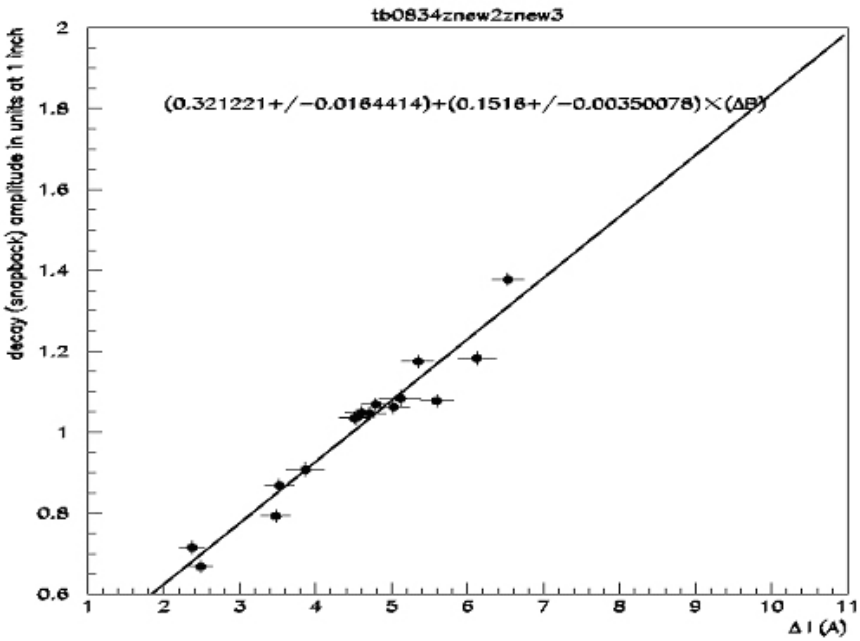

Figure 44: The snapback amplitude vs (ΔB_{snbck} ~ ΔI_{snbck}). The parametrization with (15) is shown. A constant term of ~0.32 units is observed as a result of the fit.

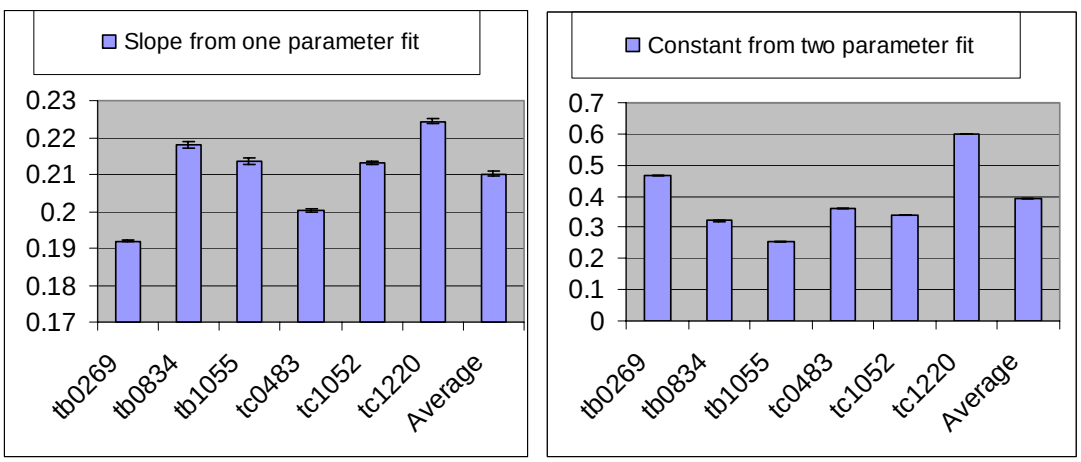

Figure 45: The values for the slope (left) and the constant term (right) for the different magnet fits with (15) are presented. The average values are shown as well.

5) Conclusions

Extensive measurements of the sextupole (b_2) component were conducted in approximately ten Tevatron dipole magnets (mostly from the spare pool). This measurement campaign included unprecedented measurements of the b_2 in the ends, and along the body of a Tevatron dipole. Also novel is a measurement of the longitudinal b_2 periodic pattern that is associated with the current imbalances that are the root cause of dynamic effects in superconducting magnets. Also for the first time, measurements of the effect of ramp-rate on the b_2 were obtained. The recent measurements were complemented with numerical models of the geometric and hysteretic b_2 components, further deepening the understanding of the sextupole in Tevatron dipoles.

In addition to the detailed measurements in select magnets, the effort was made to derive the average properties of all dipoles currently installed in the ring from the archived b_2 measurements performed in all magnets before installation in the ring. The recent progress in the understanding of dynamic effects in Tevatron dipoles also led to a better understanding of the effects of then unknown drift phenomena on the archive b_2 data. The recent measurement results in the small number of dipoles tested, were also compared to the archived results, indicating excellent agreement, a remarkable fact, given that the respective measurements were conducted more than 20 years apart with very different measurement systems.

This work has delivered important guidance for the interpretation of the beam chromaticity data obtained in dedicated Tevatron beam studies [20]. Only with a reliable knowledge of the average geometric and hysteretic b_2 components in the Tevatron can the dynamic effects in the Tevatron be properly identified. The most important aspect of the recent measurement campaign, however, was the progress made in the quantitative understanding of the magnitude and parameter dependence of b_2 drift and snapback in Tevatron dipoles. The major results of the extensive b_2 measurements on approximately ten Tevatron dipoles have been distilled into proposals for an optimization of the Tevatron operation. These proposals, discussed in further detail in [9], are:

1. Removing the pre-cycle(s) after the end of the successful store can generate an increase of integrated luminosity of up to *3%*. In such a configuration the preceding store becomes the pre-cycle of the next store and thus the pre-cycle flattops become long. The saturation of the sextupole dynamics coming from a long collision flattop leads to the additional benefits of eliminating the flattop duration parameter from the dynamic b_2 correction fit and keeping the machine in a more reproducible state.
2. Fixing the duration of the backporch will decrease further the number of parameters accountable for the compensation of the decay and snapback and thus will eliminate the effect of variations in the snapback amplitude and time. An increased duration of 5 min on the back-porch was proposed to compensate the increase in drift slope caused by the longer flattop in the pre-cycle resulting from proposal 1.

3. Decreasing the number of pre-cycles following an unintentionally ended store from six to one while increasing its flattop to *40-45 min* will not lengthen the Tevatron shot procedure but promises to bring the Tevatron into a more reproducible state.

An improved parametrization for the b_2 decay and snapback in the Tevatron will use:

4. the proposed Gaussian form (12) for the snapback compensation rather than the currently used form (11) which does not properly reflect the correlation between drift amplitude at the start of the snapback and the duration of the snapback.
5. the modified logarithmic form (10) for the decay correction during the injection plateau.

Note, however, that the dynamic effects were measured in a statistically insignificant sub-set of the Tevatron dipole magnet population. Therefore, the results obtained can only be a guide to the understanding of the Tevatron behavior. The finalized proposals for improvements of the Tevatron b_2 correction scheme will need to involve dedicated beam chromaticity measurements. These have also been conducted and are reported in [9] and [20].

References

1 G. Annala et al., "*Tevatron Dipole Measurements at MTF*", write-up of 1996 magnetic measurements on magnets TC0504 and TC1052, http://www-bdnew.fnal.gov/tevatron/adcon/magnets.html

2 D. Finley, D.A. Edwards, R.W. Hanft, R. Johnson, A.D. McInturff, J. Strait, "*Time Dependent Chromaticity Changes in the Tevatron*", PAC 12 March 1987, Washington

3 D.A. Herrup et al., "*Time Variations of Fields in Superconducting Magnets and their Effects on Accelerators*", Proceedings of the 1988 Applied Superconductivity Conference, IEEE Transactions on Magnetics, Vol. 25, No. 2, 1643-1646, March 1989 (also available as Fermilab Technical Memo TM-1543)

4 P. Bauer, "*Historical Review of the Discovery of dynamic Effects in Tevatron Magnets*", Fermilab, Technical Division Internal note TD-03-007, Feb. 2003

5 W. Fischer, "*Beam Losses on the Tevatron Ramp*", Tevatron note, see http://www-bdnew.fnal.gov/beam-physics-studies/Notes/index.htm, July 2002

6 X.L. Zang, F. Zimmermann, "*Tevatron Study Report: Pbar Tunes & Losses vs Chromaticity*", Tevatron note, see http://www-bdnew.fnal.gov/beam-physics-studies/Notes/index.htm, Jan 2003

7 M. Martens, Presentation on the Tevatron Status given to the Fermilab Accelerator Advisory Committee on February 4th, 2003 http://beamdocs.fnal.gov/DocDB/0004/000464/001/AAC_Review03_Tev_ver_final.pdf

8 T. Sen, J. Annala, P. Lebrun, R. Moore, V. Shiltsev, M. Syphers, W. Fischer, F. Schmidt, F. Zimmermann, "*Beam losses at injection energy and during acceleration in the Tevatron*", Proceedings of the 2003 Particle Accelerator Conference, Portland, U.S.A and Fermilab note Conf-03-100-T, June 2003

9 P. Bauer et al., "*Analysis of the b2 Correction in the Tevatron*", Fermilab, Technical Division Internal Note TD-03-008 Revision I, March 2003 / Sept. 2004

10 M. Haverkamp, "*Decay and Snapback in Superconducting Accelerator Magnets*", PhD Thesis, UT Twente, Netherlands, 2003

11 A. Verweij, "*Electrodynamics of Superconducting Cables for Particle Accelerator Magnets*", PhD Thesis, UT Twente, Netherlands, 1998

12 P. Bauer, L. Bottura, M. Lamm, G. Velev, "*Report on First Magnetic Measurements on Tevatron Dipole Using CERN Hall Probe Array*", Fermilab, Technical Division, internal note TD-03-011, April 2003

13 J. DiMarco, H. Glass, P. Schlabach, C. Sylvester, J. Tompkins, J. Krzywinski, *"Influence of mechanical vibrations on the field quality measurements of LHC interaction region quadrupole magnets*", IEEE Transactions on Applied Superconductivity, Volume: 10, Issue: 1, pp 1458 – 1461, March 2000

14 L. Bottura et al., "*A Fast Sextupole Probe For Snapback Measurement in the LHC Dipoles*", Proceedings of the MT 16 conference, Sept. 1999, Jacksonville, USA

15 P. Bauer et al., *"Tevatron Magnetic Models – Geometric and Hysteretic Multipoles in the Tevatron Dipole – Revision 2 April 2004"*, Fermilab, Technical Division, Internal note TD-02-040 – Revision 2, January 03

16 A. Ghosh, M. Kuchnir, "Magnetization measurements of some superconducting Cables", Fermilab Technical Memo TM-1286, Dec 14 1984

17 D.E. Johnson and D.A. Herrup "*Compensation of time Varying Field in the Tevatron Superconducting Magnets*", Proceedings of the PAC 1989

18 K.H.Mess and P. Schmüser, CERN Accelerator School on Superconductivity in Particle Accelerators, CERN Report 89-04, 1989

19 W.Fisher, A. Jain and S.Tepikian, "*Beam-Based Measurements of Persistent Current Decay in RHIC*", Phys. Rev. ST Accel. Beams 4, 2001

20 M. Martens, G. Annala, P. Bauer, D. Still, G. Velev, "Tevatron chromaticity and tune drift and snapback studies report", Fermilab/AD/TeV internal note Beams-doc-1236, Sept. 2004

APPENDIX 1

The magnet ramp implementation in the Tevatron power control module TECAR is in terms of beam energy with:

$$E(GeV) = E_{ini}(GeV) + \left(\frac{dE}{dt}\right)\Delta t(\sec) + \frac{1}{2}\left(\frac{d^2E}{dt^2}\right)(\Delta t(\sec))^2$$

The magnet ramp implementation in Fermilab's MTF is in terms of magnet current with:

$$I(A) = I_{ini}(A) + \left(\frac{dI}{dt}\right)\Delta t(\sec) + \frac{1}{2}\left(\frac{d^2I}{dt^2}\right)(\Delta t(\sec))^2$$

Table 12 gives the parameters of the current run II Tevatron ramp cycle for both implementations. The table covers exactly one cycle from 90 GeV – 980 GeV – 90 GeV, including a 1 minute dwell time at 150 GeV (injection, extraction) on both the up- and down-ramp. The real Tevatron protocol uses such a pre-cycle (with a ~20 min flat-top) followed by a cycle with a much longer injection porch (~0.5 – 2 hrs) and store at flat-top (10-20 hrs).

Table 12: Ramp parameters for standard Tevatron pre-ramp cycle between 90 GeV (reset) and 980 GeV (flat-top), including a dwell at flat-top (20 min) and the 150 GeV injection/extraction porch (1 min). The parameters refer to the above equations. The conversion to magnet current was made on the basis of the equality 980 GeV = 4332.57 A.

Nr	t_{ini}	t_{fin}	Δt	E_{ini}	E_{fin}	dE/dt	d^2E/dt^2	I_{ini}	I_{fin}	dI/dt	d^2I/dt^2
#	(sec)	(sec)	(sec)	(GeV)	(GeV)	(GeV/s)	(GeV/s^2)	(A)	(A)	(A/s)	(A/s^2)
1	0	0.5	0.5	90	94	0	32	397.91	415.6	0	141.5
2	0.5	3.752	3.254	94	146.06	16	0	415.6	645.7	70.75	0
3	3.752	4.254	0.5	146.06	150.06	16	-32	645.7	665.4	70.75	-141.5
4	**4.254**	**64.254**	**60**	**150.06**	**150.06**	**0**	**0**	**665.4**	**665.4**	**0**	**0**
5	64.254	69.665	5.411	150.06	153.09	0	0.20698	665.4	676.8	0	0.915
6	69.665	75.266	5.601	153.09	162.5	1.12	0.19999	676.8	718.5	4.952	0.884
7	72.266	78.411	6.145	162.5	180	2.24	0.19789	718.5	795.8	9.903	0.875
8	78.411	83.411	5	180	200	3.456	0.2176	795.8	884.24	15.28	0.962
9	83.411	97.713	14.302	200	300	4.544	0.34712	884.24	1326.3	20.09	1.534
10	97.713	106.623	8.9095	300	400	9.44	0.40047	1326.3	1768.4	41.74	1.770
11	106.623	113.642	7.0185	400	500	13.008	0.35337	1768.4	2210.5	57.5	1.563
12	113.642	119.994	6.3516	500	600	15.488	0.08063	2210.5	2652.6	68.47	0.356
13	119.994	142.807	22.813	600	965	16	0	2652.6	4266.2	70.75	0
14	142.807	144.682	1.875	965	980	16	-8.5333	4266.2	4332.6	70.5	-37.73
15	**144.682**	**1344.682**	**1200**	**980**	**980**	**0**	**0**	**4332.6**	**4332.6**	**0**	**0**
16	1344.682	1346.557	1.875	980	965	0	-8.53333	4332.6	4266.2	0	-37.73
17	1346.557	1369.37	22.813	965	600	-16	0	4266.2	2652.6	-70.75	0
18	1369.37	1375.722	6.3516	600	500	-16	0.08059	2652.6	2210.5	-70.75	0.356
19	1375.722	1382.741	7.0185	500	400	-15.488	0.35334	2210.5	1768.4	-68.47	1.563
20	1382.741	1391.651	8.9095	400	300	-13.008	0.40047	1768.4	1326.3	-57.5	1.770
21	1391.651	1405.953	14.302	300	200	-9.44	0.342328	1326.3	884.2	-41.74	1.534

22	1405.953	1410.953	5	200	180	-4.544	0.2176	884.2	795.8	-20.07	0.962
23	1410.953	1417.098	6.1447	180	162.5	-3.456	0.197895	795.8	718.5	-15.28	0.875
24	1417.098	1428.259	11.161	162.5	150	-2.24	0.200704	718.5	665.4	-9.903	0.887
25	**1428.259**	**1488.259**	**60**	**150**	**150**	**0**	**0**	**665.4**	**665.4**	**0**	**0**
26	1488.259	1502.322	14.063	150	105	0	-0.45508	665.4	464.6	0	-2.012
27	1502.322	1507.010	4.6875	105	90	-6.4	1.36533	464.6	397.91	-28.3	6.036

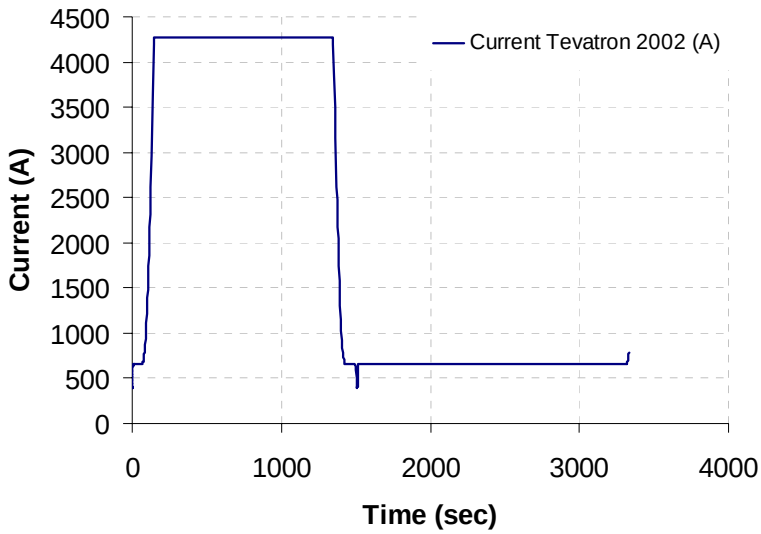

Figure 46: 2002 Tevatron magnet study standard magnet current ramp cycle. The pre-cycle corresponds to the standard Tevatron pre-cycle.